J. Fluid Mech. (1993), *vol.* 254, *pp.* 79–112

On the motion of bubbles in a periodic box

By PETER SMEREKA
Department of Mathematics, University of California, Los Angeles, CA 90024-1555, USA

(Received 18 February 1992 and in revised form 17 February 1993)

The motion of spherical bubbles in a box containing an incompressible and irrotational liquid with periodic boundary conditions is studied. Equations of motion are deduced using a variational principle. When the bubbles have approximately the same velocity their configuration is Lyapunov stable, provided they are arranged in such a way so as to minimize the effective conductivity of a composite material where the bubbles are treated as insulators. The minimizing configurations become asymptotically stable with the addition of gravity and liquid viscosity. This suggests that a randomly arranged configuration of bubbles, all with approximately the same velocity, cannot be stable. Explicit equations of motion for two bubbles are deduced using Rayleigh's method for solving Laplace's equation in a periodic domain. The results are extended for more than two bubbles by considering pairwise interactions. Numerical simulations with gravity and liquid viscosity ignored show the bubbles form clusters if initially they are randomly arranged with identical velocities. The clustering is inhibited, however, if the initial velocities are sufficiently different. The variance of the bubbles' velocities is observed to act like a temperature; a lesser amount of clustering occurs with increasing temperature. Finally, in considering the effects of gravity and liquid viscosity, the long time behaviour is found to result in the formation of bubble clusters aggregated in a plane perpendicular to the direction of gravity.

1. Introduction

In an effort to understand void wave propagation in bubbly flow, attention has been directed to the motion of rigid spherical gas bubbles in an incompressible and irrotational liquid. Many investigators have reported bubbly flows to have void waves travelling at a well-defined speed (see, for example, Pauchon & Banerjee (1986) and the references therein). The speed of these waves has been found to be almost independent of frequency, suggesting that the behaviour of void wave propagation in bubbly flow is governed by a hyperbolic system with little or no dispersion. For this reason, effective equations which describe the behaviour of averaged quantities such as void fraction or velocity are expected to be hyperbolic.

Traditionally effective equations have been derived by volume averaging the conservation laws of each phase so as to produce conservation laws for the averaged quantities (e.g. Delhaye & Achard 1976; Banerjee & Chan 1980). This leads to closure problems, however, as information is lost in the averaging procedure and constitutive relationships must be found to close the system. Since the derivation of these constitutive relationships in bubbly flow has the added difficulty of an unknown configuration of bubbles, it is typically assumed that the bubbles are arranged in a random isotropic pattern. Biesheuvel & van Wijngaarden (1984), Drew & Wood (1985) and Pauchon & Banerjee (1986), amongst others, have derived effective equations in this manner for bubbly flow, although the models presented in these papers differ because of the investigators choice of constitutive relationships.

Geurst (1985, 1986) derived effective equations using a different approach. Rather than volume averaging the conservation laws he chose to volume average the energy. The effective equations then follow from a variational principle with the volume averaged energy as the Lagrangian. This approach only requires the introduction of one phenomenological function and this can be accurately calculated. Wallis (1989) examined Geurst's model and compared it to the models of Drew & Wood (1985) and Pauchon & Banerjee (1986) and found only Geurst's model to be consistent with the motion of a single bubble. Pauchon & Smereka (1992) also studied Geurst's model and showed it to be, under suitable assumptions, equivalent to effective equations derived by volume averaging the conservation laws for each phase.

Although Geurst's model seems to have a sound theoretical basis, it turns out to be ill-posed in the dilute limit. This means the system is unstable and the effective equations are elliptic rather than hyperbolic, clearly in disagreement with experimental findings. Geurst (1985) was aware of this deficiency and showed that higher-order corrections to the phenomenological function could stabilize his model. He argued heuristically this would correspond to non-isotropic bubbly flows. It should be pointed out that both Lhuillier (1985) and van Beek (1982) obtained similar results using different approaches; van Beek associating the ill-posedness with the clustering of bubbles.

Wallis (1989) showed the phenomenological function introduced by Geurst could be related to the effective conductivity of a composite material containing a uniform conductor with embedded insulating spheres. Smereka & Milton (1991) continued this line of reasoning and demonstrated that any homogeneous arrangement of bubbles would lead to ill-posed equations. They proved, however, that if the bubbles arrange themselves in ellipsoidal clusters, the effective equations become hyperbolic over a wide range of parameter values. They do not offer a mechanism to explain how the bubbles will move into clumps.

Recently, Biesheuvel & Gorissen (1990) and van Wijngaarden & Kapteyn (1990) studied bubbly flow using ideas from the kinetic theory of gases. Biesheuvel & Gorissen derived effective equations using ensemble averages, although they too found it necessary to assume the form of several constitutive relations to close the system and obtained results similar to those found by Batchelor (1988). Van Wijngaarden & Kapteyn studied steady travelling waves in bubbly flow. They considered the dynamics of a pair of bubbles and extended their results to a suspension of bubbles considering only pairwise interactions. They also performed experiments which were found to be in reasonably close agreement with their theory.

In this paper we consider bubbly mixtures of massless, rigid, identical spheres immersed in an invicid incompressible liquid. The situation of interest is a bubbly mixture of infinite extent with no boundaries at infinity. The liquid and bubbles are initially at rest, with the bubbles then set impulsively into motion. This means that the liquid velocity is irrotational and entirely determined by the bubble motion. This system is difficult to study because there is an infinite number of bubbles to track. Therefore we turn to a more modest problem and replace the infinite bubble field by a finite collection of bubbles in a box with periodic boundary conditions on the velocity potential. Our finite collection of bubbles will retain the essential features of the infinite field. Each bubble will feel the effects of an infinite number of bubbles through the periodic images, and the liquid velocity will be entirely determined by the bubble motion. It should be noted that the periodicity of the velocity potential does not preclude the possibility of a mean flow of liquid. In fact, if the bubbles are moving roughly in the same direction, we shall see that there is necessarily a mean flow.

The goal of this paper will be to find what configuration the bubbles will take after being started from a random initial arrangement. Once it is understood how the bubbles arrange themselves, it may be possible to deduce constitutive relationships which will lead to well-posed effective equations. In §2 the equations of motion for bubbles in a box with periodic boundary conditions are derived using a variational principle as outlined in Lamb (1932). This system is then shown to conserve the kinetic energy of the liquid and its momentum. These two conserved quantities are used to construct a Lyapunov function. We use this function to prove that if the initial velocities of the bubbles are nearly the same, and their initial configuration is sufficiently close to a minimizer of the effective conductivity, then the configuration is Lyapunov stable. In the conductivity problem considered here, the bubbles are treated as insulators and the liquid has unit conductivity. It is then demonstrated that if liquid viscosity and gravity are included, all initial conditions will result in the bubbles having identical velocities and arranged so as to minimize the effective conductivity as time tends to infinity. The effects of liquid viscosity are modelled using a single-bubble model.

In §3 we compute the approximate equations of motion for two bubbles by solving Laplace's equation in a periodic box. The conditionally convergent sums that result are evaluated using a method devised by Rayleigh (1892). The results are found to agree with those of van Wijngaarden (1976, 1982) in the appropriate limits. A two-bubble model accounting for liquid viscosity, similar to the model derived by Kok (1988), is included. In §4 the two-bubble model is extended to more bubbles by considering pairwise interactions. The approximations used in §§3 and 4 are similar in many respects to those used by van Wijngaarden & Kapteyn (1990).

The numerical results are presented in §5. In the conservative case, it is observed that the bubbles have a strong tendency to form clusters which are positioned broadside to the direction of flow. This clustering is inhibited, however, by the variance of the bubble's velocities. If the variance is sufficiently large, clustering is prohibited and a random homogeneous configuration will persist. The effects of gravity and liquid viscosity cause the bubbles to arrange themselves ultimately into pancake-shaped clumps oriented broadside to the direction of flow.

2. General theory

The equations of motion are obtained using a variational principle as outlined in Lamb (1932, chapter 4). A set of ordinary differential equations is given describing the location of the centre of each bubble.

2.1. *Equations of motion*

We take the liquid velocity, $\boldsymbol{v}_l$, to be irrotational; thus

$$\boldsymbol{v}_l = \nabla\phi, \tag{2.1}$$

where ϕ is the velocity potential. Since the liquid is incompressible, ϕ satisfies Laplace's equation

$$\nabla^2\phi = 0. \tag{2.2}$$

The normal component of the liquid velocity is equal to the normal component of the bubble's velocity on its surface, thereby giving the boundary conditions:

$$\frac{\partial\phi}{\partial n} = \boldsymbol{u}_k \cdot \boldsymbol{n}, \quad \text{for } k = 1 \text{ to } N, \tag{2.3}$$

where $\boldsymbol{u}_k$ is the velocity of the kth bubble and $\boldsymbol{n}$ is the outward drawn normal from the liquid surface into the bubble. We shall take ϕ to be periodic on the box. The boundary conditions are imposed by first writing ϕ as

$$\phi = \sum_{k=1}^{N} \boldsymbol{u}_k \cdot \boldsymbol{\Psi}_k, \tag{2.4}$$

where $\boldsymbol{\Psi}_k$ is a vector-valued function associated with the kth bubble. $\boldsymbol{\Psi}_k$ is determined entirely by the positions of the bubbles and its components must be harmonic. The boundary conditions are satisfied by taking

$$\frac{\partial \psi_{k,\alpha}}{\partial n} = \begin{cases} n_\alpha & \text{on the } k\text{th sphere,} \\ 0 & \text{on the other spheres,} \end{cases} \tag{2.5}$$

for $\alpha = x$, y and z. Here, subscript α denotes the components of the vectors, i.e.

$$\boldsymbol{\Psi}_k = \psi_{k,x}\boldsymbol{e}_x + \psi_{k,y}\boldsymbol{e}_y + \psi_{k,z}\boldsymbol{e}_z, \tag{2.6}$$

where $\boldsymbol{e}_x$, $\boldsymbol{e}_y$ and $\boldsymbol{e}_z$ are unit vectors along the x-, y- and z-axes, respectively. Clearly (2.4) combined with (2.5) will satisfy (2.2) and (2.3). The periodicity condition is respected by taking $\psi_{k,\alpha}$ to be periodic. The physical interpretation of (2.5) shows the kth bubble moving with unit velocity in the n_α direction while the other bubbles remain stationary.

The kinetic energy of the liquid is:

$$T = \tfrac{1}{2}\rho_l \int_{V_l} |\nabla\phi|^2 \, \mathrm{d}V, \tag{2.7}$$

where ρ_l is the liquid density and V_l is the region of the cube occupied by the liquid. Using Green's theorem, we have

$$T = \tfrac{1}{2}\rho_l \sum_{k=1}^{N} \int_{S_k} \phi \frac{\partial \phi}{\partial n} \mathrm{d}S_k + \tfrac{1}{2}\rho_l \int_{\partial V} \phi \frac{\partial \phi}{\partial n} \mathrm{d}S, \tag{2.8}$$

where S_k denotes the surface of the kth sphere and ∂V denotes the boundary of the box. The integration over ∂V is zero by periodicity. Substituting (2.4) into (2.8), we obtain

$$T = \tfrac{1}{2}\rho_l \sum_{k=1}^{N} \int_{S_k} \left(\sum_i \boldsymbol{u}_i \cdot \boldsymbol{\Psi}_i\right)\left(\sum_j \frac{\partial}{\partial n}(\boldsymbol{u}_j \cdot \boldsymbol{\Psi}_j)\right) \mathrm{d}S_k. \tag{2.9}$$

The above equation simplifies, when we use (2.5), to

$$T = \tfrac{1}{2}\rho_l \sum_{i,j} \boldsymbol{u}_i \cdot \int_{S_j} \boldsymbol{\Psi}_i \boldsymbol{n} \, \mathrm{d}S_j \cdot \boldsymbol{u}_j, \tag{2.10}$$

where the sum is understood to run from $i = 1$ to N and $j = 1$ to N. Now we define the matrix

$$\boldsymbol{A}_{ij} = \int_{S_j} \boldsymbol{\Psi}_i \boldsymbol{n}^T \, \mathrm{d}S_j, \tag{2.11}$$

where the superscript T denotes the transpose and $\boldsymbol{A}_{ij}$ is a 3×3 matrix for each i and j. The entries of $\boldsymbol{A}_{ij}$ depend only on the positions of the bubbles and not on their velocities. This follows from the boundary conditions on the $\boldsymbol{\Psi}_k$. The matrices $\boldsymbol{A}_{ij}$ remain unchanged if the bubbles are rigidly translated together. Later we shall see that this invariance will give rise to conservation of momentum.

The matrices $\boldsymbol{A}_{ij}$ have the following properties:

$$\boldsymbol{A}_{ij} = \boldsymbol{A}_{ji} \quad \text{(symmetric)}, \tag{2.12a}$$

$$\boldsymbol{A}_{ij} = \boldsymbol{A}_{ij}^T \quad \text{(self-adjoint)}. \tag{2.12b}$$

First we will establish (2.12*a*). Using (2.5) and the periodicity condition, we can write

$$\boldsymbol{A}_{ij} = \int_{S+\partial V} \boldsymbol{\Psi}_i \left(\frac{\partial \boldsymbol{\Psi}_j}{\partial n}\right)^T \mathrm{d}S,$$

where $S+\partial V$means the integration is taken over al liquid surfaces (the surfaces of the spheres and the sides of the box). It follows from Green's identity and (2.5) that

$$\boldsymbol{A}_{ij} = \int_{S+\partial V} \boldsymbol{\Psi}_j \left(\frac{\partial \boldsymbol{\Psi}_i}{\partial n}\right)^T \mathrm{d}S = \int_{S_i} \boldsymbol{\Psi}_j \boldsymbol{n}^T \mathrm{d}S_i = \boldsymbol{A}_{ji}.$$

To prove (2.12*b*), we write $\boldsymbol{A}_{ij}$ in component form:

$$A_{ij,\alpha\beta} = \int_{S_j} \psi_{i\alpha} n_\beta \mathrm{d}S_j \quad (\alpha, \beta = x, y \text{ and } z).$$

We show, using similar arguments to the above, that

$$\begin{aligned} A_{ij,\alpha\beta} &= \int_{S+\partial V} \psi_{i\alpha} \frac{\partial \psi_{j\beta}}{\partial n} \mathrm{d}S, \\ &= \int_{S_i} \psi_{j\beta} \frac{\partial \psi_{i\alpha}}{\partial n} \mathrm{d}S_i, \\ &= A_{ji,\beta\alpha} = A_{ij,\beta\alpha}. \end{aligned}$$

Thus we establish (2.12*b*).

Combining (2.10) and (2.11) we find the total energy of the system is

$$T = \tfrac{1}{2}\rho_l \sum_{i,j} \boldsymbol{u}_i^T \boldsymbol{A}_{ij} \boldsymbol{u}_j, \tag{2.13}$$

where

$$\boldsymbol{A}_{ij} = \boldsymbol{A}_{ij}(\boldsymbol{x}_1, \ldots, \boldsymbol{x}_N) \quad \text{and} \quad \dot{\boldsymbol{x}}_i = \boldsymbol{u}_i. \tag{2.14}$$

Therefore $\boldsymbol{u}_i$ is a generalized velocity for the bubble's position, implying that T is the Lagrangian for the system and the equations of motion can be deduced from the Euler–Lagrange equation (see Lamb 1932, chapter 4). The Euler–Lagrange equation is

$$\frac{\mathrm{d}}{\mathrm{d}t}\frac{\partial T}{\partial \boldsymbol{u}_k} - \frac{\partial T}{\partial \boldsymbol{x}_k} = 0, \quad \text{for } k = 1 \text{ to } N. \tag{2.15}$$

Substituting (2.13) into the above expression and using (2.12*a*, *b*), we obtain

$$\frac{\mathrm{d}}{\mathrm{d}t}\sum_i \boldsymbol{A}_{ki}\boldsymbol{u}_i - \frac{1}{2}\sum_{i,j} \boldsymbol{u}_i^T \frac{\partial \boldsymbol{A}_{ij}}{\partial \boldsymbol{x}_k}\boldsymbol{u}_j = 0.$$

Since

$$\frac{\mathrm{d}}{\mathrm{d}t}\boldsymbol{A}_{ki} = \sum_j \boldsymbol{u}_j^T \frac{\partial \boldsymbol{A}_{ki}}{\partial \boldsymbol{x}_j}, \tag{2.16}$$

the previous equation becomes

$$\sum_i \boldsymbol{A}_{ki}\dot{\boldsymbol{u}}_i = \sum_{i,j} \boldsymbol{u}_i^T \left[\frac{1}{2}\frac{\partial \boldsymbol{A}_{ij}}{\partial \boldsymbol{x}_k} - \frac{\partial \boldsymbol{A}_{kj}}{\partial \boldsymbol{x}_i}\right]\boldsymbol{u}_j; \tag{2.17}$$

which, when combined with

$$\dot{\boldsymbol{x}}_k = \boldsymbol{u}_k, \tag{2.18}$$

gives us the equations of motion.

2.3. *Conserved quantities.*

It is clear that T is a conserved quantity; multiplying (2.17) by $\boldsymbol{u}_k^T$ and summing over k, we find

$$\sum_{k,i} \boldsymbol{u}_k^T \boldsymbol{A}_{ki} \dot{\boldsymbol{u}}_i = \sum_{k,i} -\boldsymbol{u}_k^T \dot{\boldsymbol{A}}_{ki} \boldsymbol{u}_i + \frac{1}{2} \sum_{i,j,k} \boldsymbol{u}_k^T \boldsymbol{u}_i^T \frac{\partial \boldsymbol{A}_{ij}}{\partial \boldsymbol{x}_k} \boldsymbol{u}_j.$$

When the last term on the right-hand side is simplified using (2.16), the above equation becomes

$$\sum_{k,i} \boldsymbol{u}_k^T \boldsymbol{A}_{ki} \dot{\boldsymbol{u}}_i + \frac{1}{2} \sum_{k,i} \boldsymbol{u}_k^T \dot{\boldsymbol{A}}_{ki} \boldsymbol{u}_i = 0.$$

Since $\boldsymbol{A}_{ki}$ is symmetric and self-adjoint, we have

$$\frac{\mathrm{d}T}{\mathrm{d}t} = 0. \tag{2.19}$$

Next we will establish conservation of momentum. In the situation we consider here, the kinetic energy of the liquid remains unchanged if the bubbles are rigidly translated. Therefore we have

$$T(\boldsymbol{x}_1, \boldsymbol{x}_2, \ldots, \boldsymbol{x}_N) = T(\boldsymbol{x}_1 + \boldsymbol{d}, \boldsymbol{x}_2 + \boldsymbol{d}, \ldots, \boldsymbol{x}_N + \boldsymbol{d}), \tag{2.20}$$

where $\boldsymbol{d}$ is an arbitrary vector. Expanding the right-hand side of (2.20), we obtain

$$T(\boldsymbol{x}_1, \boldsymbol{x}_2, \ldots, \boldsymbol{x}_N) = T(\boldsymbol{x}_1, \boldsymbol{x}_2, \ldots, \boldsymbol{x}_N) + \boldsymbol{d}^T \sum_k \frac{\partial T}{\partial \boldsymbol{x}_k} + O(d^2).$$

The above expression must be true for all orders in $\boldsymbol{d}$; thus,

$$\sum_k \frac{\partial T}{\partial \boldsymbol{x}_k} = 0. \tag{2.21}$$

If we sum (2.15) over k, we have

$$\frac{\mathrm{d}}{\mathrm{d}t} \sum_k \frac{\partial T}{\partial \boldsymbol{u}_k} = 0, \tag{2.22}$$

which shows the following quantity to be conserved:

$$\rho_l \sum_{k,i} \boldsymbol{A}_{ki} \boldsymbol{u}_i = \text{constant}. \tag{2.23}$$

This conserved quantity is the momentum of the fluid. We can verify this by directly integrating the liquid velocity over V_l. The liquid momentum is

$$\boldsymbol{M} = \rho_l \int_{V_l} \nabla \phi \, \mathrm{d}V.$$

Using Gauss's theorem, we find the components of the momentum to be

$$M_\alpha = \rho_l \int_S \phi \boldsymbol{e}_\alpha \cdot \boldsymbol{n} \, \mathrm{d}S \quad (\alpha = x, y \text{ and } z), \tag{2.24}$$

where S indicates the integral is to be taken over all of the spheres. The contributions from the sides of the cube vanish from periodicity. Substituting (2.4) into (2.24), and splitting the integration up among the spheres, we find

$$M_\alpha = \rho_l \boldsymbol{e}_\alpha \cdot \sum_k \int_{S_k} \left(\sum_j \boldsymbol{\Psi}_j^T \boldsymbol{u}_j \right) \boldsymbol{n} \, \mathrm{d}S_k,$$

$$= \rho_l \boldsymbol{e}_\alpha \cdot \sum_{j,k} \int_{S_k} \boldsymbol{n} \boldsymbol{\Psi}_j^T \, \mathrm{d}S_k \boldsymbol{u}_j,$$

$$= \rho_l \boldsymbol{e}_\alpha \cdot \sum_{j,k} \boldsymbol{A}_{jk}^T \boldsymbol{u}_j.$$

Since $\boldsymbol{A}_{jk}$ is self-adjoint, we have

$$\boldsymbol{M} = \rho_l \sum_{j,k} \boldsymbol{A}_{jk} \boldsymbol{u}_j. \tag{2.25}$$

Thus the total liquid momentum is a conserved quantity, showing that, in general, the mean liquid velocity is not zero. It should be mentioned that $\boldsymbol{M}$ is also the total impulse or 'virtual momentum' of the system and is the same as the actual momentum because of the periodic boundary conditions.

2.4. *Stability of bubble configurations*

In this section, we consider the stability of certain arrangements of bubbles with approximately the same velocity. Here we shall see that if the bubbles are arranged in such a way so as to minimize, or closely minimize, the effective conductivity in the direction of the liquid momentum, the configuration will be Lyapunov stable.

2.4.1. *Construction of the Lyapunov function*

To begin we shall decompose the bubble's velocity as follows:

$$\boldsymbol{u}_k = \boldsymbol{c} + \boldsymbol{w}_k, \tag{2.26}$$

such that

$$\sum_{i,j} \boldsymbol{A}_{ij} \boldsymbol{w}_j = 0, \tag{2.27}$$

which implies that $\boldsymbol{c}$ satisfies

$$\rho_l \mathscr{A} \boldsymbol{c} = \boldsymbol{M}, \tag{2.28}$$

where

$$\mathscr{A} = \sum_{i,k} \boldsymbol{A}_{ik}.$$

The above relationship shows that if all the bubbles have the same velocity, $\boldsymbol{c}$ the momentum of the liquid will be $\boldsymbol{M}$. The relationship between $\boldsymbol{M}$ and $\boldsymbol{c}$ has been explored by Wallis (1989) and Smereka & Milton (1991). They show that for bubbles moving with identical velocities, and with periodic boundary conditions on the velocity potential,

$$\boldsymbol{M} = V \mathscr{K} \boldsymbol{c}, \tag{2.29}$$

where $\mathscr{K}$ is the energy coefficient matrix:

$$\mathscr{K} = \rho_l [(1-\epsilon) \boldsymbol{I} - \boldsymbol{\sigma}]. \tag{2.30}$$

Here $\boldsymbol{I}$ is the identity matrix, ϵ is the void fraction and $\boldsymbol{\sigma}$ is the effective conductivity

matrix of a material where the spheres are taken as insulators and the liquid has unit conductivity. From (2.28) and (2.29), we find that

$$\left(\frac{\mathscr{A}^{-1}}{\rho_l}-\frac{\mathscr{K}^{-1}}{V}\right)\boldsymbol{M}=0.$$

This must be true for any $\boldsymbol{M}$ since the liquid momentum can be in any direction; thus,

$$\mathscr{A}=\frac{V}{\rho_l}\mathscr{K}. \tag{2.31}$$

If we substitute (2.26) into (2.13), and use (2.27), (2.28) and (2.31), we find

$$T=\frac{1}{2V}\boldsymbol{M}^T\mathscr{K}^{-1}\boldsymbol{M}+\tfrac{1}{2}\rho_l\sum_{i,j}\boldsymbol{w}_i^T\boldsymbol{A}_{ij}\boldsymbol{w}_j. \tag{2.32}$$

This form of the kinetic energy is notable as the first term depends only on the position of the bubbles, consequently it is an effective potential energy. For convenience we write

$$\mathscr{U}=\frac{1}{2V}\boldsymbol{M}^T\mathscr{K}^{-1}\boldsymbol{M} \tag{2.33}$$

and

$$T'=\tfrac{1}{2}\rho_l\sum_{i,j}\boldsymbol{w}_i^T\boldsymbol{A}_{ij}\boldsymbol{w}_j, \tag{2.34}$$

where $\mathscr{U}$ is the effective potential energy and T' is the effective kinetic energy. Let us now consider configuration of bubbles that satisfy the variational principle

$$\min'\mathscr{U}, \tag{2.35}$$

where min′ indicates minimizing over $\boldsymbol{x}_k$ with $|\boldsymbol{x}_i-\boldsymbol{x}_j|>2a$ for all $i\neq j$. This inequality ensures that the bubbles will not overlap. We expect these configurations to be stable since they are minima (either local or global) of the effective potential energy.

$\mathscr{U}$ is minimized when the bubbles are arranged so as to minimize the effective conductivity in the direction of $\boldsymbol{M}$. To prove this we take $\boldsymbol{M}=M\boldsymbol{e}_z$, without loss of generality, and obtain

$$\mathscr{U}=\frac{M^2}{2V}\boldsymbol{e}_z^T\mathscr{K}^{-1}\boldsymbol{e}_z. \tag{2.36}$$

Computing the inverse of $\mathscr{K}$, we find that

$$\mathscr{U}=\frac{M^2}{2V}\frac{1}{(\mathscr{K}_{zz}-Q)}, \tag{2.37}$$

where

$$Q=\frac{\mathscr{K}_{yy}\mathscr{K}_{xz}^2-2\mathscr{K}_{xy}\mathscr{K}_{xz}\mathscr{K}_{yz}+\mathscr{K}_{xx}\mathscr{K}_{yz}^2}{\mathscr{K}_{xx}\mathscr{K}_{yy}-\mathscr{K}_{xy}^2},$$

and the subscripted $\mathscr{K}$ terms are the components of $\mathscr{K}$. The denominator of Q is a minor of $\mathscr{K}$ and since $\mathscr{K}$ is positive definite then $\mathscr{K}_{xx}\mathscr{K}_{yy}-\mathscr{K}_{xy}^2>0$. From this it is possible to show that

$$Q\geqslant 0,$$

and

$$Q=0, \quad \text{if and only if} \quad \mathscr{K}_{xz}=\mathscr{K}_{yz}=0.$$

It is clear from (2.37) that $\mathscr{U}$ is minimized by maximizing $\mathscr{K}_{zz}$ and minimizing Q. For any configuration of bubbles, $\mathscr{K}_{xz}$ and $\mathscr{K}_{yz}$ can always be made zero by an appropriate rigid rotation of the configuration. The minimum value of Q will consequently be zero and such a rotation will necessarily extremize $\mathscr{K}_{zz}$. It therefore follows from (2.30) that

the configurations which minimize $\mathscr{U}$ can be found with the following variational principle:

$$\min' \sigma_{zz}. \tag{2.38}$$

The configurations which satisfy this variational principle are not unique for two reasons: first, any rigid translate of a minimizer is also a minimizer and, secondly, the effective potential energy may have several local minima.

It is interesting to compare (2.38) with a result in Lamb (1932, Art. 128) concerning the stability of a translating ellipsoid. It is shown that the ellipsoid is stable only if it is travelling in such an orientation so as to maximize its virtual mass. This means it will be stable if it is broadside to its direction of travel. Evidently, from (2.29), the analogy of the virtual mass tensor for periodic structures is $V\mathscr{K} = V\rho_l[\boldsymbol{I}(1-\boldsymbol{\epsilon})-\boldsymbol{\sigma}]$, and the direction of travel is $\boldsymbol{M}$. The virtual mass in the direction of $\boldsymbol{M}$ is

$$\frac{V}{M^2}\boldsymbol{M}^T\mathscr{K}\boldsymbol{M}. \tag{2.39}$$

Hence the variational principle given by (2.38) can be equivalently expressed as

$$\max' \{\text{virtual mass}\}. \tag{2.40}$$

Finally, it should be mentioned that (2.40) is similar to the variational principle deduced by Benjamin (1987) for a single bubble with surface tension. Benjamin, however, considers variations of the bubble's shape, and here we consider variations of the bubbles' configuration.

2.4.2. *Stability result*

If the bubbles are placed in a configuration that is sufficiently close to a minimizer of σ_{zz}, if their initial velocities are all sufficiently similar, and the liquid momentum is in the z-direction then the configuration will stay close, modulo a rigid translate, to its initial arrangement for all time.

To prove this we need to introduce some notation. We will denote the spatial configuration of the bubbles at a time t as $\mathscr{C}(t) = \{\boldsymbol{x}_1, \boldsymbol{x}_2, \ldots, \boldsymbol{x}_N\}$ and a configuration that satisfies (2.38) as $\mathscr{C}_m$. Next we consider

$$|\mathscr{U}[\mathscr{C}(t)]-\mathscr{U}(\mathscr{C}_m)| \tag{2.41}$$

and minimize it over all configurations that satisfy (2.38). A configuration that minimizes (2.41) is denoted $\mathscr{C}_m^*(t)$. Certainly this is not unique since $\mathscr{U}$ will not change if the bubbles are rigidly translated together. Therefore $\mathscr{T}[\mathscr{C}_m^*(t)]$ will also minimize (2.41) where $\mathscr{T}[\cdot]$ denotes any rigid translate of the bubbles. $\mathscr{T}[\mathscr{C}_m^*(t)]$ is the solution of (2.38) that is closest to $\mathscr{C}(t)$, where (2.41) is used as the measure of closeness.

Now consider a collection of bubbles that at time zero is arranged in a configuration $\mathscr{C}(0)$ and given velocities $\boldsymbol{u}_k$ for $k = 1$ to N, which are decomposed as given by (2.26). Since T is a constant of the motion, we have

$$T'(t)+\mathscr{U}(\mathscr{C}(t))-\mathscr{U}(\mathscr{T}[\mathscr{C}_m^*(0)]) = \delta_1+\delta_2, \tag{2.42}$$

where $\delta_1 = T'(0)$ and $\delta_2 = \mathscr{U}(\mathscr{C}(0))-\mathscr{U}(\mathscr{T}[\mathscr{C}_m^*(0)])$. The constants δ_1 and δ_2 can be made as small as we like by choice of initial conditions. If the bubbles have nearly the same velocity δ_1 is small. Since $\mathscr{T}[\mathscr{C}_m^*(0)]$ is a minimizer of $\mathscr{U}$ then $\mathscr{U}(\mathscr{C}(t))-\mathscr{U}(\mathscr{T}[\mathscr{C}_m^*(0)]) > 0$ for $\mathscr{C}(t)$ in a neighbourhood of $\mathscr{T}[\mathscr{C}_m^*(0)]$. This implies that $T'(t)+\mathscr{U}(\mathscr{C}(t))-\mathscr{U}(\mathscr{T}[\mathscr{C}_m^*(0)])$ can be used as a Lyapunov function. The initial configuration will stay close to $\mathscr{T}[\mathscr{C}_m^*(0)]$ for all time if δ_1 and δ_2 are sufficiently small. $\mathscr{T}[\mathscr{C}_m^*(0)]$ is close to $\mathscr{T}[\mathscr{C}(0)]$ since δ_2 is small.

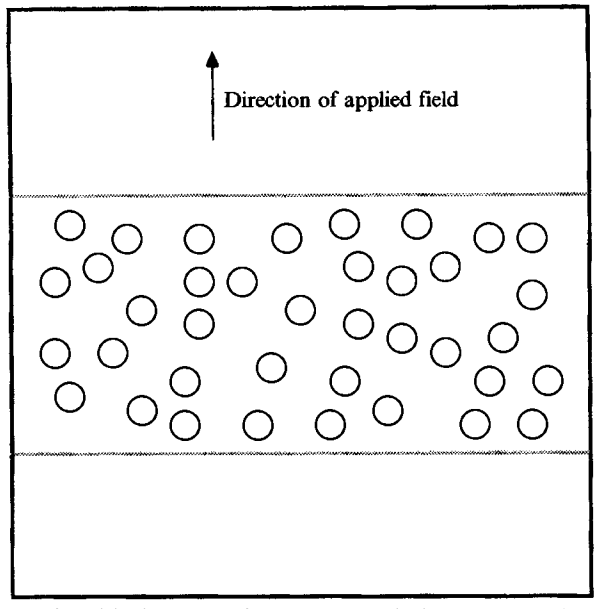

FIGURE 1. An example of an idealized non-homogeneous bubbly flow is pictured here. The bubbles are randomly arranged inside the two dotted lines. The conductivity will be lowered as the distance between the two lines is reduced.

2.4.3. *Description of stable configurations*

Consider a box containing only two bubbles. From Jeffrey (1973), we know that σ_{zz} will be a minimum if the two bubbles are touching with their line of centre perpendicular to the z-axis. If more bubbles are added then we expect σ_{zz} to be lowest when all the bubbles are tightly packed in a single plane perpendicular to the z-axis (see figure 3).

Now suppose there is a very large number of bubbles arranged as shown in figure 1. If we further suppose that the bubbles are arranged inside the slab in a random fashion, we obtain

$$\sigma_{zz} = \frac{p-\epsilon}{p+\epsilon(\frac{3}{2}p-1)}, \tag{2.43}$$

where p is the fraction of the mixture that contains bubbles. Equation (2.43) is obtained by considering the media to be three regions placed 'in series'. The regions containing no bubbles have unit conductivity and the region containing bubbles assumes the conductivity of a composite material composed of a random suspension of insulating spheres in a media of unit conductivity. Differentiating (2.43) shows

$$\frac{\partial \sigma_{zz}}{\partial p} > 0, \tag{2.44}$$

which means the conductivity must decrease as p decreases, thereby indicating the minimum will occur when p is as small as possible. The fact that the spheres are not allowed to overlap ensures $p > \epsilon$. This shows that a stable configuration for a large number of bubbles is a tightly packed slab perpendicular to the z-axis.

2.4.4. *Discussion*

The results of this section can be interpreted using basic ideas from the mechanics of conservative systems. If such a system is started close to a minimum of its potential energy, with small kinetic energy, it will stay close to its original position. In our case, this corresponds to the bubbles being given approximately the same velocity (small effective kinetic energy) and arranged in a tightly packed horizontal slab (close to a minimum of the effective potential energy).

The situation is more complicated if one starts a conservative system far from a minimum of the potential energy and with no kinetic energy. Typically, one would expect the system to move initially toward a potential energy minimum and thereby gain kinetic energy. For later times it is difficult to determine what would happen, especially for a system with a large number of degrees of freedom. It is likely that the system would wander around a minimum of the potential energy. For interacting particle systems, one can expect a partitioning between the kinetic and potential energy when the system is in statistical equilibrium. This means the time average of the potential energy would be less than its initial value and the kinetic energy would be correspondingly higher.

In considering the bubbles, we can start far from a minimum of the effective potential energy by taking a random homogeneous arrangement of bubbles. The effective kinetic energy will be small when the bubbles are given approximately the same velocity. In view of the paragraph above, we would expect that when the bubbles are in statistical equilibrium the time average of the potential energy will be lower than its initial value. The only way that this can occur is if the bubbles cluster to some degree. This suggests that if given similar velocities the bubbles have a propensity to cluster.

2.5. *Effects of gravity and liquid viscosity*

We shall take gravity to be the z-direction pointing downwards so that $\boldsymbol{g} = -g\boldsymbol{e}_z$. The force on a single bubble due to gravity is

$$\rho_l \tau g \boldsymbol{e}_z. \tag{2.45}$$

We shall use a simplified model to include the effects of viscosity. Rather than accurately model the viscous effects, our goal here is to include a mechanism for the dissipation of energy. We shall assume the viscous effects occur in a thin boundary layer around the bubble and model the viscous force as

$$12\pi\mu a[\boldsymbol{u}_k - \boldsymbol{v}_l(\boldsymbol{x}_k)], \tag{2.46}$$

where μ is the viscosity of the liquid and $\boldsymbol{v}_l(\boldsymbol{x}_k)$ is the ambient liquid velocity at the centre of kth bubble. The first term in (2.46) can be found in Batchelor (1967), amongst others, and the correction for the mean flow is due to Levich (1962). Later we shall see that because of the boundary conditions on ϕ, $\boldsymbol{v}_l(\boldsymbol{x}_k)$ falls off as R^{-3}, where R is the distance between bubbles. The leading-order term in (2.46), then, is

$$12\pi\mu a \boldsymbol{u}_k. \tag{2.47}$$

For the present discussion, the viscous force will be modelled with (2.47) and we will return to (2.46) later. The body force on kth bubble is found by adding (2.45) to (2.47). The equations of motion accounting for gravity and liquid viscosity are

$$\frac{\mathrm{d}}{\mathrm{d}t}\frac{\partial T}{\partial \boldsymbol{u}_k} - \frac{\partial T}{\partial \boldsymbol{x}_k} = \rho_l \tau g \boldsymbol{e}_z - 12\pi\mu a \boldsymbol{u}_k, \tag{2.48}$$

where T is given by (2.13). From computations similar to those in §2, it follows that

$$\frac{\mathrm{d}T}{\mathrm{d}t} = \rho_l g \tau \boldsymbol{e}_z^T \sum_k \boldsymbol{u}_k - 12\pi\mu a \sum_k |\boldsymbol{u}_k|^2, \tag{2.49}$$

and

$$\frac{\mathrm{d}\boldsymbol{M}}{\mathrm{d}t} = -12\pi\mu a \sum_k (\boldsymbol{u}_k - \boldsymbol{u}_\infty), \tag{2.50}$$

where

$$\boldsymbol{u}_\infty = u_\infty \boldsymbol{e}_z, \quad u_\infty = \frac{\rho_l a^2 g}{9\mu}. \tag{2.51}$$

u_∞ is the rise speed of a single bubble (see Batchelor 1967, §5.14). If we multiply (2.50) by $\boldsymbol{u}_\infty^T$ and subtract it from (2.49), we obtain

$$\frac{\mathrm{d}}{\mathrm{d}t}(T - \boldsymbol{u}_\infty^T \boldsymbol{M}) = -12\pi\mu a \sum_k |\boldsymbol{u}_k - \boldsymbol{u}_\infty|^2. \tag{2.52}$$

We let $\boldsymbol{v}_k = \boldsymbol{u}_k - \boldsymbol{u}_\infty$ and find

$$\frac{\mathrm{d}\mathscr{F}}{\mathrm{d}t} = -12\pi\mu a \sum_k |\boldsymbol{v}_k|^2, \tag{2.53}$$

where

$$\mathscr{F} = -\tfrac{1}{2}u_\infty^2 \boldsymbol{e}_z^T \mathscr{K} \boldsymbol{e}_z + \tfrac{1}{2}\rho_l \sum_{i,j} \boldsymbol{v}_i^T \boldsymbol{A}_{ij} \boldsymbol{v}_j.$$

Clearly $\mathscr{F}$ will decrease on all trajectories for which $|\boldsymbol{v}_k| \neq 0$. Therefore, as $t \to \infty$, all trajectories must tend to minimizers of $\mathscr{F}$. Since the second term of $\mathscr{F}$ is positive definite, the minimizers have $\boldsymbol{v}_k = 0$ for all k. The final configuration of the bubbles must satisfy the variational principle

$$\max' \boldsymbol{e}_z^T \mathscr{K} \boldsymbol{e}_z, \tag{2.54}$$

which is equivalent to (2.38). This implies that the configurations which satisfy (2.38) are asymptotically stable. It also demonstrates, within the context of this simple model, that the combined effect of gravity and viscosity causes all initial conditions to tend to clustered slabs where all the bubbles are moving with the same velocity. Later we shall see that a similar behaviour occurs when the effects of liquid viscosity are modelled with (2.46).

3. The two-bubble problem

In this section, the equations of motion will be computed using the point-bubble approximation for two bubbles. This approximation considers only the dipole fields and consequently is only quantitatively valid when the bubbles are far apart. Nevertheless, some results based on work of Basset (1887) will be presented, which indicate that this approximation is appropriate even when the bubbles collide.

3.1. *Computation of* $\boldsymbol{A}_{ij}$

The goal of this section is to compute an expression for the $\boldsymbol{A}_{11}$, $\boldsymbol{A}_{12}$, and $\boldsymbol{A}_{22}$ using the point-bubble approximation. Determination of these quantities will allow explicit equations of motion to be determined using (2.17). We consider two bubbles inside a cube of length L. We use a rectangular coordinate system (x', y', z') and place the two spheres with their centres on the z'-axis, and use a pair of spherical coordinates (r_1, θ_1, ϕ) and (r_2, θ_2, ϕ) with the origins being at spheres 1 and 2 respectively. The ϕ coordinate is common to both systems. To locate the spheres to an arbitrary position

within the cube, the coordinate system is first rotated by an angle α in the (y', z')-plane, followed by a rotation of β in the transformed (x', y')-plane. This generates a new coordinate system denoted by (x, y, z). The sides of the cube are parallel to the x-, y- and z-axes. The transformation matrix between (x, y, z) and (x', y', z') is

$$\boldsymbol{P} = \begin{pmatrix} \cos\beta & -\cos\alpha\sin\beta & \sin\alpha\sin\beta \\ \sin\beta & \cos\alpha\cos\beta & -\sin\alpha\cos\beta \\ 0 & \sin\alpha & \cos\alpha \end{pmatrix}. \tag{3.1}$$

The derivation of $\boldsymbol{A}_{11}\boldsymbol{e}_z$ and $\boldsymbol{A}_{12}\boldsymbol{e}_z$ is presented below. The other columns of these matrices are computed in a similar fashion. From (2.11), we have

$$\boldsymbol{A}_{1j}\boldsymbol{e}_z = \int_{S_j} \psi_{1z}\boldsymbol{n}\,\mathrm{d}S_j \quad \text{for } j = 1, 2, \tag{3.2}$$

where ψ_{1z} is the harmonic function that is periodic on the cube and satisfies the boundary conditions given by (2.5):

$$\frac{\partial\psi_{1z}}{\partial n} = \begin{cases} n_z & \text{on sphere 1,} \\ 0 & \text{on sphere 2.} \end{cases} \tag{3.3}$$

We look for a solution of the form

$$\psi_{1z} = G(\boldsymbol{r}) + \frac{A_1 a^3}{2r_1^2}\cos\theta_1 + \frac{B_1 a^3}{2r_1^2}\sin\theta_1\sin\phi + \frac{C_1 a^3}{2r_1^2}\sin\theta_1\cos\phi\ldots,$$
$$+ \frac{A_2 a^3}{2r_2^2}\cos\theta_2 + \frac{B_2 a^3}{2r_2^2}\sin\theta_2\sin\phi + \frac{C_2 a^3}{2r_2^2}\sin\theta_2\cos\phi\ldots, \tag{3.4}$$

where A_1, A_2, B_1, B_2, C_1 and C_2 are constants to be determined and a is the radius of the sphere. $G(\boldsymbol{R})$ is the harmonic function containing the growing spherical harmonics, and therefore arises from sources outside the cell. These are the fields created by the periodic images of the two bubbles and later we shall see that $G(\boldsymbol{R})$ is $O(R^{-3})$. To apply the boundary conditions we must expand ψ_{1z} near the two spheres. This is done with the following expansions

$$\frac{\cos\theta_2}{r_2^2} \approx \frac{1}{R^2} + \frac{2r_1\cos\theta_1}{R^3}, \tag{3.5a}$$

$$\frac{\sin\theta_2}{r_2^2} \approx \frac{r_1\sin\theta_1}{R^3}. \tag{3.5b}$$

Similar relations are found by interchanging 1 and 2 in (3.5a) and (3.5b). The behaviour of ψ_{1z} near S_i is

$$\psi_{1z} = G(S_i) + \nabla G(S_i)\cdot\boldsymbol{r} + \left(\frac{A_i}{2r_i^2} + \frac{A_{3-i}r_i}{R^3}\right)a^3\cos\theta_i$$
$$+ \left(\frac{B_i}{2r_i^2} + \frac{B_{3-i}r_i}{2R^3}\right)a^3\sin\theta_i\sin\phi + \left(\frac{C_i}{2r_i^2} + \frac{C_{3-i}r_i}{2R^3}\right)a^3\sin\theta_i\cos\phi + \ldots, \tag{3.6}$$

where $G(S_i)$ and $\nabla G(S_i)$ are G and its gradient, evaluated at the centre of S_i, $i = 1$ and 2. Applying the boundary conditions at sphere 1 shows

$$\begin{pmatrix} C_1 - \dfrac{a^3}{2R^3} C_2 \\ B_1 - \dfrac{a^3}{2R^3} B_2 + \sin\alpha \\ A_1 - \dfrac{a^3}{R^3} A_2 + \cos\alpha \end{pmatrix} \approx \boldsymbol{P}^T \nabla G(S_1),$$

and at sphere 2,

$$\begin{pmatrix} C_2 - \dfrac{a^3}{2R^3} C_1 \\ B_2 - \dfrac{a^3}{2R^3} B_1 \\ -A_1 + \dfrac{a^3}{R^3} A_1 \end{pmatrix} \approx \boldsymbol{P}^T \nabla G(S_2).$$

Solving for the unknowns, we find

$$(C_1, B_1, A_1) \approx (0, -\sin\alpha, -\cos\alpha) + \nabla G(S_1)^T \boldsymbol{P},$$

$$(C_2, B_2, -A_2) \approx \left(0, -\frac{a^3}{2R^3}\sin\alpha, \frac{a^3}{R^3}\cos\alpha\right) + \nabla G(S_2)^T \boldsymbol{P}.$$

Substituting the expressions for A_i, B_i and C_i into (3.6), we obtain

$$\boldsymbol{A}_{11} \boldsymbol{e}_z = \int_{S_1} \psi_{1z} \boldsymbol{n} \, \mathrm{d}S \approx -\tfrac{3}{2}\tau \nabla G(S_1) + (0, 0, \tfrac{1}{2}\tau)^T, \tag{3.7}$$

$$\boldsymbol{A}_{12} \boldsymbol{e}_z = \int_{S_2} \psi_{1z} \boldsymbol{n} \, \mathrm{d}S \approx -\tfrac{3}{2}\tau \nabla G(S_2) - \tfrac{3}{4}\tau \frac{a^3}{R^3} \begin{pmatrix} 3R_x R_z/R^2 \\ 3R_y R_z/R^2 \\ -1 + 3R_z^2/R^2 \end{pmatrix}. \tag{3.8}$$

The value of ∇G, evaluated at the centres of S_1 and S_2, is deduced using crucial observation made by Rayleigh (1892): that the growing parts of the velocity potential must arise from exterior effects, namely the field produced by the spheres outside the reference cell. This field is also approximated by the point-bubble model. The contribution made by sphere 1 in the qth cell is

$$\phi_q = -\tfrac{1}{2}a^3 \frac{z - z_q}{r_q^3},$$

where $r_q^2 = (x - x_q)^2 + (y - y_q)^2 + (z - z_q)^2$ and (x_q, y_q, z_q) is the coordinate of the centre of sphere 1 in the qth cell. The contribution made by sphere 2 is zero to the accuracy of this approximation. Using Rayleigh's observation, we have

$$G(r) \approx \sum_{|q|=1}^{\infty} \phi_q, \tag{3.9}$$

where $\Sigma_{|q|=1}$ indicates the sum is to be taken over all periodic images of the reference

cell. Taking the gradient of both sides of (3.9), and evaluating it at the centre of S_i, we obtain

$$\nabla G(S_i) = a^3(\Sigma_{ix}, \Sigma_{iy}, \Sigma_{iz})^T,$$

where

$$\left.\begin{aligned}
\Sigma_{1x} &= \frac{3}{2}\sum_{|q|=1}^{\infty}\frac{(\boldsymbol{\rho}_q\cdot\boldsymbol{e}_x)(\boldsymbol{\rho}_q\cdot\boldsymbol{e}_z)}{\rho_q^5}, \quad \Sigma_{1y} = \frac{3}{2}\sum_{|q|=1}^{\infty}\frac{(\boldsymbol{\rho}_q\cdot\boldsymbol{e}_y)(\boldsymbol{\rho}_q\cdot\boldsymbol{e}_z)}{\rho_q^5},\\
\Sigma_{1z} &= \frac{1}{2}\sum_{|q|=1}^{\infty}\frac{1}{\rho_q^3}\left(\frac{3(\boldsymbol{\rho}_q\cdot\boldsymbol{e}_z)^2}{\rho_q^2}-1\right), \quad \Sigma_{2x} = \frac{3}{2}\sum_{|q|=1}^{\infty}\frac{(\boldsymbol{R}_q\cdot\boldsymbol{e}_x)(\boldsymbol{R}_q\cdot\boldsymbol{e}_z)}{R_q^5},\\
\Sigma_{2y} &= \frac{3}{2}\sum_{|q|=1}^{\infty}\frac{(\boldsymbol{R}_q\cdot\boldsymbol{e}_y)(\boldsymbol{R}_q\cdot\boldsymbol{e}_z)}{R_q^5}, \quad \Sigma_{2z} = \frac{1}{2}\sum_{|q|=1}^{\infty}\frac{1}{R_q^3}\left(\frac{3(\boldsymbol{R}_q\cdot\boldsymbol{e}_z)^2}{R_q^2}-1\right).
\end{aligned}\right\} \tag{3.10}$$

Here $\boldsymbol{\rho}_q$ is the vector joining sphere 1 in the reference cell and its image in the qth cell, and $\boldsymbol{R}_q$ is the vector joining sphere 1 in the reference cell and sphere 2 in the qth cell.

Since these lattice sums do not converge absolutely, their sum depends on how the terms are added. Rayleigh (1892) discusses this problem and offers a solution. His result was generalized by McPhedran & McKenzie (1978). Σ_{1z} is $L^{-3}S_2$, where S_2 is the sum in Rayleigh's paper and is equal to $\frac{2}{3}\pi$. The other sums can also be evaluated using this method. Σ_{1x} and Σ_{1y} are found to be zero and

$$\left.\begin{aligned}
\Sigma_{2x} &= \frac{3}{2}\sum_{|q|=1}^{\infty}{}^{\bigstar}\frac{(\boldsymbol{R}_q\cdot\boldsymbol{e}_x)(\boldsymbol{R}_q\cdot\boldsymbol{e}_z)}{R_q^5}\\
\Sigma_{2y} &= \frac{3}{2}\sum_{|q|=1}^{\infty}{}^{\bigstar}\frac{(\boldsymbol{R}_q\cdot\boldsymbol{e}_y)(\boldsymbol{R}_q\cdot\boldsymbol{e}_z)}{R_q^5}\\
\Sigma_{2z} &= \frac{2\pi}{3L^3}+\frac{1}{2}\sum_{|q|=1}^{\infty}{}^{\bigstar}\frac{1}{R_q^3}\left(\frac{3(\boldsymbol{R}_q\cdot\boldsymbol{e}_z)^2}{R_q^2}-1\right),
\end{aligned}\right\} \tag{3.11}$$

where the $\bigstar$ indicates the sum is to be added up with cubic symmetry about the reference cell. Combining the above expressions for $\nabla G(S_i)$, and applying the above method to find the other columns of $\boldsymbol{A}_{ij}$, we find

$$\boldsymbol{A}_{11} = \boldsymbol{A}_{22} = \tfrac{1}{2}\tau\left(1-\frac{3}{2}\frac{\tau}{L^3}\right)\boldsymbol{I}, \tag{3.12a}$$

$$\boldsymbol{A}_{12} = \boldsymbol{A}_{21} = -\frac{3}{4}\frac{\tau^2}{L^3}\boldsymbol{I}+\tfrac{3}{4}\tau\sum_{q=0}^{\infty}{}^{\bigstar}\frac{a^3}{R_q^3}\left(\boldsymbol{I}-3\frac{\boldsymbol{R}_q\boldsymbol{R}_q^T}{R_q^2}\right), \tag{3.12b}$$

where $\boldsymbol{I}$ is the identity matrix and $\boldsymbol{R}_0 = \boldsymbol{R}$.

3.2. *Motion of two bubbles in an unbounded liquid*

To compare (3.12) with previous results, we must consider the case of an unbounded liquid. Taking $L\to\infty$, we have

$$\boldsymbol{A}_{11} = \boldsymbol{A}_{22} = \tfrac{1}{2}\tau\boldsymbol{I} \tag{3.13a}$$

and

$$\boldsymbol{A}_{12} = \boldsymbol{A}_{21} = \tfrac{3}{4}\tau\frac{a^3}{R^3}\left(\boldsymbol{I}-3\frac{\boldsymbol{R}\boldsymbol{R}^T}{R^2}\right). \tag{3.13b}$$

The total energy is

$$T = \tfrac{1}{4}\rho_l\left(|\boldsymbol{u}_1|^2+|\boldsymbol{u}_2|^2+3\frac{a^3}{R^3}\left[\boldsymbol{u}_1\cdot\boldsymbol{u}_2-3\frac{(\boldsymbol{u}_1\cdot\boldsymbol{R})(\boldsymbol{u}_2\cdot\boldsymbol{R})}{R^2}\right]\right). \tag{3.14}$$

Let us now consider two special cases of (3.14) in which the bubbles have velocities $\boldsymbol{u}_1 = \boldsymbol{u}_2 = U\boldsymbol{e}_z$. In the first case, they are moving perpendicular to their line of centres so that $\boldsymbol{R} \cdot \boldsymbol{e}_z = 0$, therefore

$$T = \tfrac{1}{2}\rho_l\left(1+\frac{3}{2}\frac{a^3}{R^3}\right)U^2. \tag{3.15}$$

In the second case, the bubbles are moving parallel to their line of centres. Thus $\boldsymbol{R} \cdot \boldsymbol{e}_z = R$ and (3.14) becomes

$$T = \tfrac{1}{2}\rho_l\left(1-3\frac{a^3}{R^3}\right)U^2. \tag{3.16}$$

Equations (3.15) and (3.16) are in agreement with the results of van Wijngaarden (1976, equations (3.18) and (3.27)).

A more generalized study of the motion of two bubbles is facilitated with the new variables $\boldsymbol{s} = \boldsymbol{x}_1 + \boldsymbol{x}_2$ and $\boldsymbol{R} = \boldsymbol{x}_1 - \boldsymbol{x}_2$. Their substitution into (3.14) gives

$$T = \tfrac{1}{4}\rho_l(\dot{\boldsymbol{s}}^T H_+ \dot{\boldsymbol{s}} + \dot{\boldsymbol{R}}^T H_- \dot{\boldsymbol{R}}), \tag{3.17}$$

where

$$H_\pm(\boldsymbol{R}) = \tfrac{1}{2}\boldsymbol{I} \pm \frac{3}{4}\frac{a^3}{R^3}\left(\boldsymbol{I}-3\frac{\boldsymbol{R}\boldsymbol{R}^T}{R^2}\right).$$

The equations of motion are given by the Euler–Lagrange equation:

$$\frac{\mathrm{d}}{\mathrm{d}t}\frac{\partial T}{\partial \dot{\boldsymbol{s}}} - \frac{\partial T}{\partial \boldsymbol{s}} = 0, \tag{3.18}$$

$$\frac{\mathrm{d}}{\mathrm{d}t}\frac{\partial T}{\partial \dot{\boldsymbol{R}}} - \frac{\partial T}{\partial \boldsymbol{R}} = 0. \tag{3.19}$$

Since $\boldsymbol{s}$ does not appear explicitly in T, (3.18) becomes

$$\frac{\mathrm{d}}{\mathrm{d}t}\frac{\partial T}{\partial \dot{\boldsymbol{s}}} = \frac{\mathrm{d}}{\mathrm{d}t}H_+\dot{\boldsymbol{s}} = 0,$$

which means

$$H_+\dot{\boldsymbol{s}} = \boldsymbol{J}, \tag{3.20}$$

where $\boldsymbol{J}$ is a constant of the motion. We solve for $\dot{\boldsymbol{s}}$ and substitute it into (3.19) and find

$$\frac{\mathrm{d}}{\mathrm{d}t}\frac{\partial T}{\partial \dot{\boldsymbol{R}}} - \dot{\boldsymbol{R}}^T\frac{\partial H_-}{\partial \boldsymbol{R}}\dot{\boldsymbol{R}} + \boldsymbol{J}^T\frac{\partial H_+^{-1}}{\partial R}\boldsymbol{J} = 0. \tag{3.21}$$

The foregoing equation has the Lagrangian

$$\mathscr{L} = \dot{\boldsymbol{R}}^T H_- \dot{\boldsymbol{R}} - \boldsymbol{J}^T H_+^{-1}\boldsymbol{J}. \tag{3.22}$$

This form of the Lagrangian has the $\dot{\boldsymbol{s}}$ dependence removed. Notice that the first term is similar to a kinetic energy, while the second depends only on $\boldsymbol{R}$ and is therefore an effective potential energy. Computing the inverse of H_+ and taking $\boldsymbol{J} = J\boldsymbol{e}_z$, we obtain

$$\boldsymbol{J}^T H_+^{-1}\boldsymbol{J} = \frac{2J^2}{\left(1+\dfrac{3a^3}{2R^3}\right)\left(1-3\dfrac{a^3}{R^3}\right)}\left(1-3\frac{a^3}{R^3}+\frac{9a^3\cos^2\theta}{2R^3}\right), \tag{3.23}$$

where θ is the angle between $\boldsymbol{R}$ and the z-axis. Since this expression is only accurate to R^{-3}, then to the same accuracy we have

$$\boldsymbol{J}^T H_+^{-1}\boldsymbol{J} = 2J^2 + \frac{3a^3J^2}{R^3}(3\cos^2\theta - 1). \tag{3.24}$$

Writing $\dot{\boldsymbol{R}}^T H_- \dot{\boldsymbol{R}}$ in spherical coordinates, and leaving out the constant term in (3.24) as it makes no contribution to the equations of motion, we have the following expression for the Lagrangian

$$\mathscr{L} = \frac{1}{2}\left(1-\frac{3}{2}\frac{a^3}{R^3}\right)(\dot{R}^2+R^2\dot{\theta}^2+R^2\sin^2\theta\dot{\phi}^2)+\frac{9a^3}{4R^3}\dot{R}^2+\frac{3a^3J^2}{R^3}(3\cos^2\theta-1). \quad (3.25)$$

If we ignore azimuthal dependence and terms of the order $|\dot{\boldsymbol{R}}|^2R^{-3}$, we recover the Lagrangian except for an unimportant constant derived by van Wijngaarden (1982). His work shows the bubbles can be either attracted to each other or repelled, depending on initial conditions. For example, if the bubbles are given the same velocity and are moving perpendicular to their line of centres, they move towards each other and collide. If, on the other hand, they are moving parallel to their line of centres, they will be repelled from each other. We find this behaviour for trajectories determined by using (3.25) in the Euler–Lagrange equation. The equations of motion for $L \neq \infty$ were computed using (3.12) substituted into (2.17), and the computed trajectories were qualitatively the same as those for $L = \infty$.

Clearly when the bubbles become too close, the approximations under which (3.14) was derived are violated although the behaviour is qualitatively correct. The bubbles are attracted as a result of the lower pressure that is between them as compared to the pressure in the surrounding fluid. This is true for any bubble separation distance, therefore one expects this behaviour will occur even if the higher order terms are included.

The accuracy of the point-bubble approximation as the bubbles move closer together is assessed using a result of Basset (1887). Consider two bubbles initially located at $\boldsymbol{r}_1 = (-x,0,0)^T$ and $\boldsymbol{r}_2 = (x,0,0)^T$, each given unit velocity in the direction of the z-axis. By symmetry, the line joining the centres of the bubbles will stay perpendicular to the z-axis and the bubbles will have velocities $\boldsymbol{u}_1 = (-\dot{x},0,\dot{z}^T)$ and $\boldsymbol{u}_2 = (\dot{x},0,\dot{z})^T$. Basset shows that the kinetic energy accurate to $O(x^{-12})$ is

$$T = \rho_l[a(x)\,\dot{x}^2+b(x)\,\dot{z}^2], \quad (3.26)$$

where
$$a(x) = \tfrac{1}{2}\tau\,[1+3\xi^3+\chi(3\xi^6+9\xi^8+3\xi^9+18\xi^{10}+18\xi^{11}+33\xi^{12})],$$
$$b(x) = \tfrac{1}{2}\tau\,[1+\tfrac{3}{2}\xi^3+\chi(\tfrac{3}{4}\xi^6+3\xi^8+\tfrac{3}{8}\xi^9+\tfrac{27}{4}\xi^{10}+3\xi^{11}+\tfrac{65}{16}\xi^{12})],$$
$$\xi = a/2x, \quad \chi = 1.$$

If we set $\chi = 0$, the point-bubble approximation is recovered. The equations of motion are deduced using (3.26) in the Euler–Lagrange equation. These are solved numerically for $\chi = 1$ and $\chi = 0$, with $a = 1$ until they touch. An example of this type of computation is shown in figure 2. The difference between the two trajectories is so small they cannot be distinguished on the graph. The maximum discrepancy is found to occur at $x = 1$, the bubbles' radii, and has a relative magnitude of 0.2%. These results suggest that the point-bubble approximation is appropriate even when the bubbles touch.

3.3. *Collision model*

In view of the prior discussion, it is clear that one must model collisions. Here a simple model will be used. It will be assumed that the bubbles bounce off each other like elastic spheres and that no coalescence occurs. First, we consider two bubbles in an unbounded liquid. The potential energy resulting from their collision is taken as

$$\phi_c = \frac{\kappa\rho_l T}{6a^3}(|R-2a|+2a-R)^3. \quad (3.27)$$

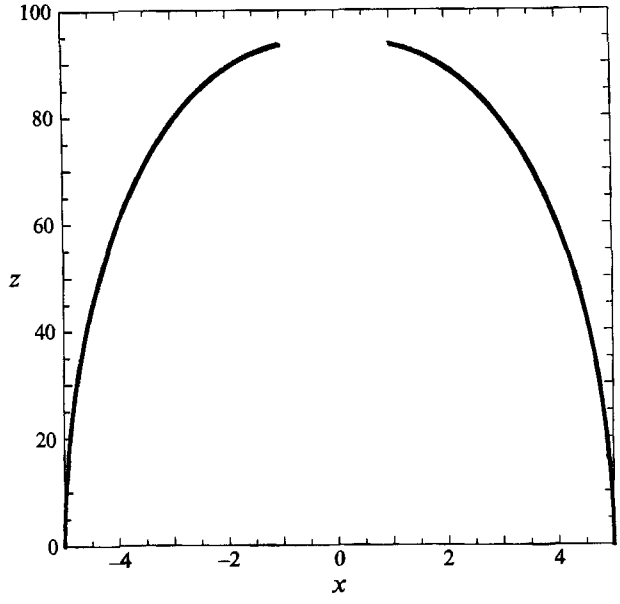

FIGURE 2. The trajectories of two bubbles using the dipole approximation and Basset's approximation are shown. The difference between the two trajectories is smaller than the line width and consequently cannot be seen.

This potential energy is zero for $R > 2$. The cubic power was chosen so as when $-\phi_c$ is added to the Lagrangian, it gives rise to a force which is differentiable in $\boldsymbol{R}$ (this will help in the numerics). To extend (3.27) to the periodic box, we have the following collision potential energy:

$$\phi_c = \frac{\kappa \rho_l \tau}{6a^3} \sum_{q=0}^{adj} (|R_q - 2a| + 2a - R_q)^3. \tag{3.28}$$

The upper limit in the sum means it is carried out over the cells adjacent to the reference cell. This ensures the bubbles properly collide with the image bubbles.

3.4. *Viscous effects*

A liquid velocity, denoted $v_l(x_1)$, is induced at the centre of sphere 1 by sphere 2 and by the images of both spheres. Using the dipole approximation, we find

$$v_l(x_1) = -\frac{2}{3\tau}[\boldsymbol{A}_{12}\boldsymbol{u}_2 + (\boldsymbol{A}_{11} - \tfrac{1}{2}\tau \boldsymbol{I})\boldsymbol{u}_1]. \tag{3.29}$$

A similar relation can be found by interchanging 1 and 2. This result combined with (2.46) shows the total viscous force on the ith bubble is

$$12\pi\mu a \sum_j \boldsymbol{D}_{ij}\boldsymbol{u}_j, \tag{3.30}$$

where

$$\boldsymbol{D}_{11} = \boldsymbol{D}_{22} = \left(1 - \frac{\tau}{2L^3}\right)\boldsymbol{I}$$

and

$$\boldsymbol{D}_{12} = \boldsymbol{D}_{21} = \frac{3}{2\tau}\boldsymbol{A}_{12}.$$

If we take $L \to \infty$, these relations can be inferred from those reported by Kok (1988).

Van Wijngaarden & Kapteyn (1990) summarized Kok's results and discussed in some depth the reason D_{12} is proportional to A_{12}.

4. Extension to N bubbles

The two-bubble problem will be extended to N bubbles by considering only pairwise interactions. This would be a good approximation for dilute well-mixed bubbly flows if the two-bubble problem had been solved exactly. Since the two-bubble problem was solved using the point-bubble approximation, we are formally restricted to dilute well-separated mixtures. Nevertheless, in view of the dynamics deduced from (3.26), we can also expect good accuracy for well-mixed suspensions. If any clustering occurs, the accuracy of this approach will not be clear. There is, however, no reason why we should not expect qualitative agreement, especially in view of the results contained in §4.2 below. Van Wijngaarden & Kapteyn (1990) also used the point-bubble approximation to study the dynamics of bubble pairs which were extended to bubbly flows considering pairwise interactions. They studied steady void wave propagation in bubbly flows and found reasonably good agreement with their experiments. This lends more evidence to the validity of the point-bubble approximation.

We shall denote the vector joining the centres of the ith and jth bubbles in the reference cell as $\boldsymbol{R}_{ij}$. The vector that joins the ith sphere in the reference cell to the jth sphere in the qth cell is denoted $\boldsymbol{R}_{ij,q}$. Therefore we have

$$\boldsymbol{A}_{ii} = \tfrac{1}{2}\tau\left(1-\frac{3}{2}\frac{\tau}{L^3}\right)\boldsymbol{I}, \tag{4.1a}$$

and for $i \neq j$

$$\boldsymbol{A}_{ij} = -\frac{3}{4}\frac{\tau^2}{L^3}\boldsymbol{I}+\tfrac{3}{4}\tau\sum_{q=0}^{\infty}{}^{\star}\frac{a^3}{R_{ij,q}^3}\left(\boldsymbol{I}-3\frac{\boldsymbol{R}_{ij,q}\boldsymbol{R}_{ij,q}^T}{R_{ij,q}^2}\right). \tag{4.1b}$$

Similar relations are also found for $\boldsymbol{D}_{ij}$. The potential energy for the collisions is

$$\phi_c = \frac{\kappa\rho_l\tau}{6a^3}\sum_{\substack{i,j\\ i\neq j}}\sum_{q=0}^{adj}(|R_{ij,q}-2a|+2a-R_{ij,q})^3. \tag{4.2}$$

4.1. *Equations of motion*

The Lagrangian for the bubbles, including the collision model, is $\mathscr{L} = T-\phi_c$. The Euler–Lagrange equation is

$$\sum_i \boldsymbol{A}_{ki}\dot{\boldsymbol{u}}_i = \sum_{i,j}\boldsymbol{u}_i^T\left[\frac{1}{2}\frac{\partial \boldsymbol{A}_{ij}}{\partial \boldsymbol{x}_k}-\frac{\partial \boldsymbol{A}_{kj}}{\partial \boldsymbol{x}_i}\right]\boldsymbol{u}_j-\frac{\partial\phi_c}{\partial \boldsymbol{x}_k}+\boldsymbol{f}_k, \tag{4.3}$$

where $\boldsymbol{f}_k$ are the forces on the bubble due to gravity and liquid viscosity:

$$\boldsymbol{f}_k = -12\pi\mu a\sum_i \boldsymbol{D}_{ik}\boldsymbol{u}_i+\rho_l\tau g\boldsymbol{e}_z. \tag{4.4}$$

The equations of motion are found by substituting the expressions for $\boldsymbol{A}_{ij}$ and $\boldsymbol{D}_{ij}$ into (4.3). Before explicit equations of motion are computed, let us write the equations in dimensionless form. The following variables will be used:

$$\boldsymbol{x}_k = a\tilde{\boldsymbol{x}}_k, \quad \boldsymbol{u}_k = u_\infty\tilde{\boldsymbol{u}}_k, \quad t = \frac{a}{u_\infty}\tilde{t}, \tag{4.5}$$

where the ˜ denotes dimensionless variables. We substitute (4.5) into (4.3) and (4.4), and then drop the tildes to obtain

$$\tfrac{1}{2}\dot{\boldsymbol{u}}_k+\frac{18}{Re}\boldsymbol{u}_k+\sum_j \boldsymbol{C}_{jk}\left(\dot{\boldsymbol{u}}_j+\frac{12}{Re}\boldsymbol{u}_j\right)=\frac{18}{Re}\boldsymbol{e}_z+\boldsymbol{f}_{ck}+\sum_{\substack{j\\ j\neq k}}\sum_{q=0}^{\infty}{}^{\star}\frac{1}{R_{jk,q}^5}$$
$$\left(\tfrac{9}{2}(\boldsymbol{u}_j^T\boldsymbol{R}_{kj,q})\boldsymbol{u}_j+\tfrac{9}{4}|\boldsymbol{u}_j|^2\boldsymbol{R}_{kj,q}-\tfrac{45}{4}(\boldsymbol{u}_j^T\boldsymbol{R}_{kj,q})^2\frac{\boldsymbol{R}_{kj,q}}{R_{kj,q}^2}\right), \quad (4.6)$$

where
$$\boldsymbol{C}_{ij}=\begin{cases}-\dfrac{\pi}{L^3}\boldsymbol{I} & (i=j),\\ -\dfrac{\pi}{L^3}\boldsymbol{I}+\dfrac{3}{4}\sum_{q=0}^{\infty}{}^{\star}\dfrac{1}{R_{ij,q}^3}\left(\boldsymbol{I}-3\dfrac{\boldsymbol{R}_{ij,q}\boldsymbol{R}_{ij,q}^T}{R_{ij,q}^2}\right) & (i\neq j),\end{cases}$$

$$\boldsymbol{f}_{ck}=\kappa\sum_{\substack{i\\ i\neq k}}\sum_{q=0}^{adj}(|R_{ki,q}-2|+2-R_{ki,q})^2\boldsymbol{R}_{ki,q}/R_{ki,q},$$

and $Re=2au_\infty\rho_l/\mu$ is the Reynolds number of a single bubble. If we let $Re\to\infty$, we recover the case with no gravity and no liquid viscosity.

4.2. *Stable configurations*

In the previous section we established that if $Re=\infty$, then a configuration was stable if sufficiently close to a minimizer of effective conductivity. In this section, we shall find an approximate expression for σ_{zz} and then numerically compute minimizing configurations. From (2.31) we known that

$$\sigma_{zz}=1+\epsilon-\frac{1}{V}\sum_{i,j}\boldsymbol{e}_z^T\boldsymbol{A}_{ij}\boldsymbol{e}_z, \quad (4.7)$$

and using the expression for $\boldsymbol{A}_{ij}$ in dimensionless form, we obtain

$$\sigma_{zz}\approx\sigma_{zz}^{(a)}=1-\tfrac{3}{2}\epsilon+\tfrac{3}{4}\epsilon^2+\frac{3\epsilon}{2N}\sum_{\substack{i,j\\ i\neq j}}\sum_{q=0}^{\infty}{}^{\star}\frac{P_2\{\cos(\theta_{ij,q})\}}{R_{ij,q}^3}, \quad (4.8)$$

where P_2 is the second Legendre polynomial and $\theta_{ij,q}$ is the angle between $\boldsymbol{R}_{ij,q}$ and $\boldsymbol{e}_z$. Arguments similar to those in §2.4 show that stable solutions of (4.6) with $Re=\infty$ satisfy

$$\min{}'\,\sigma_{zz}^{(a)}.$$

Bubble configurations that minimize $\sigma_{zz}^{(a)}$, with the constraint that the bubbles cannot overlap, were computed using an IMSL optimization routine called *bcong*. Figure 3 shows an example of such a calculation for 27 bubbles with $L=15$. The left-hand side of the figure shows the 'guess' or starting point, while the right-hand side shows a minimizing configuration. Figure 3 clearly shows the bubbles clustering in a plane perpendicular to the z-axis to lower the effective conductivity. It should be noted that the location of the bubble cluster is completely arbitrary and any translate is also a minimizer. It is natural to speculate on what would happen if we use more bubbles than the number that fills a horizontal plane. The results of such a situation are presented in figure 4, where we started with 125 bubbles and $L=15$. The 'guess' configuration was a randomly perturbed simple cubic lattice and the minimizing arrangement clearly shows the bubbles clustering into single tightly packed slab.

$\sigma_{zz}^{(a)}$ may have several local minima in addition to its global minimum; therefore

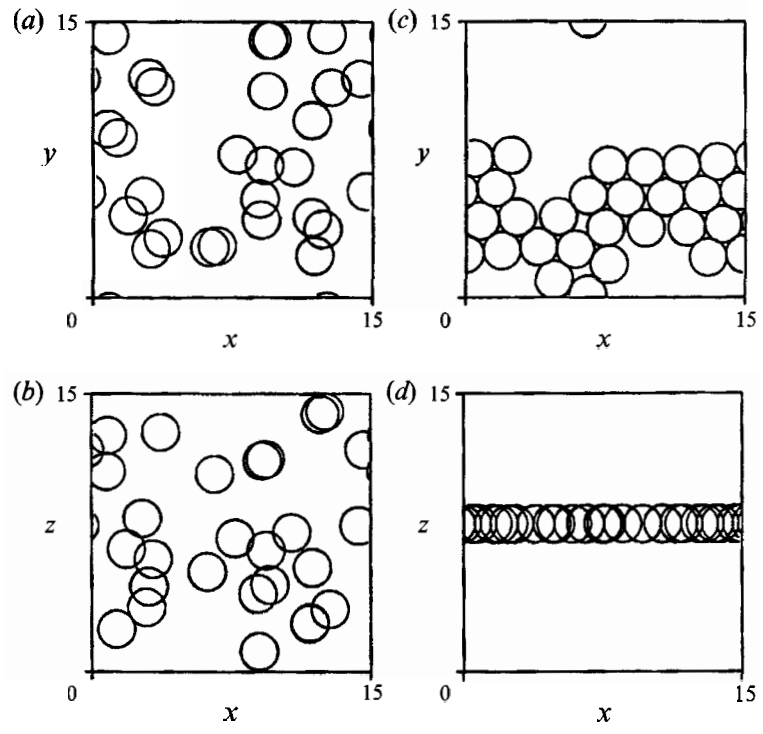

FIGURE 3. An arrangement of 27 bubbles that minimize σ_{zz}. (*a*) and (*b*) show the initial guess, in the (x,y)- and (x,z)-planes, respectively; (*c*) and (*d*) show the corresponding minimizer.

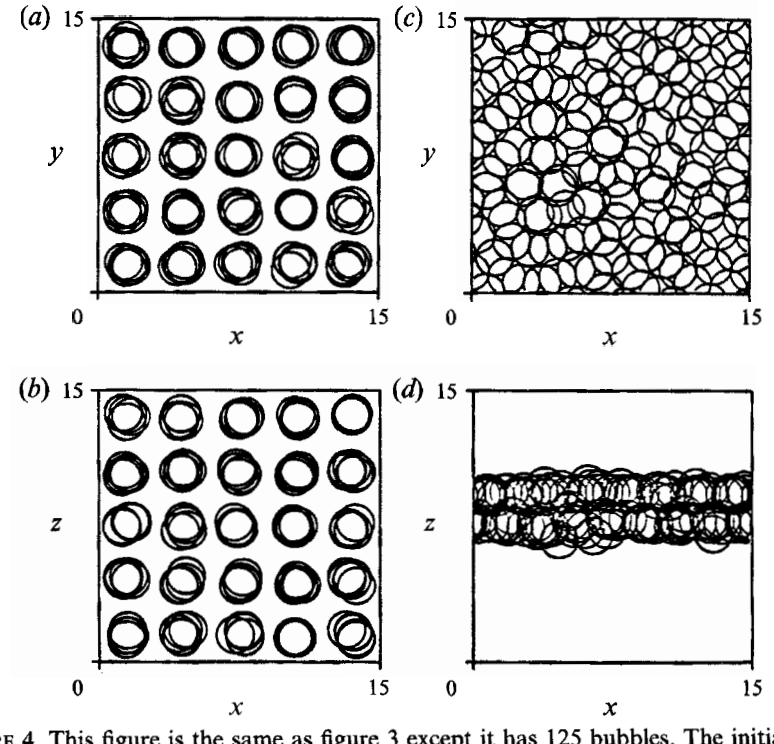

FIGURE 4. This figure is the same as figure 3 except it has 125 bubbles. The initial guess was a small random perturbation of a simple cubic lattice.

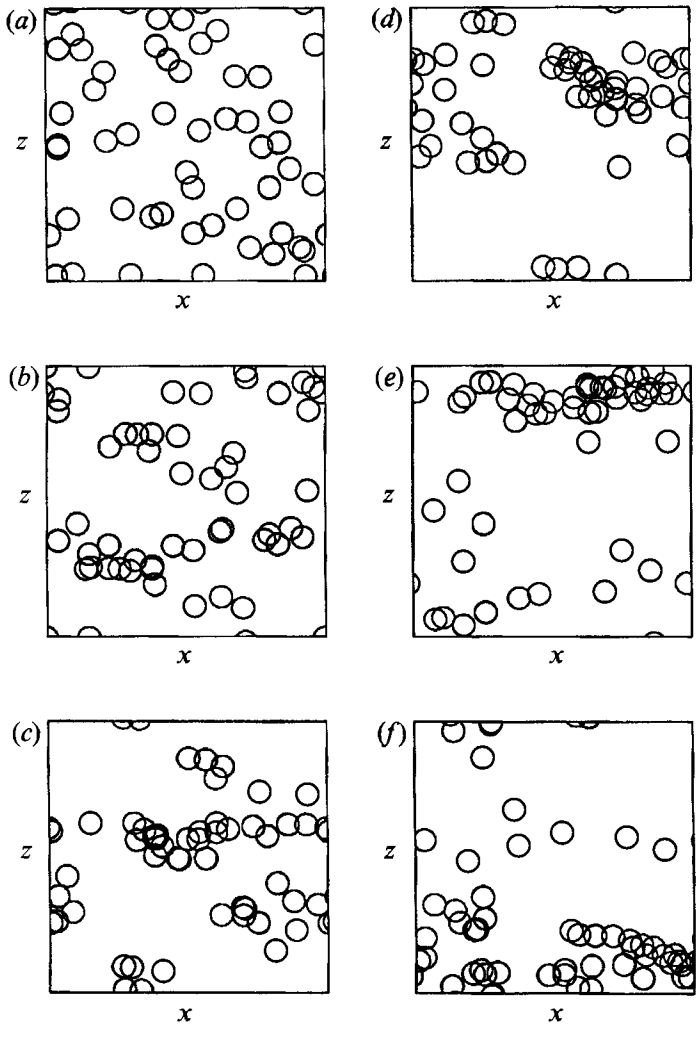

FIGURE 5. Various snapshots are shown of the evolution of 50 bubbles, with $L = 25$. The bubbles started from a random configuration with unit velocity in the z-direction are shown. This figure presents the projection onto the (x, z)-plane. The snapshot times are: $(a) = 0$, $(b) = 36$, $(c) = 72$, $(d) = 108$, $(e) = 144$, $(f) = 180$.

these stable solutions may not be unique. When $Re \neq \infty$ we expect the bubbles to asymptotically tend to a minimizer of $\sigma_{zz}^{(a)}$. Since the minimizers may not be unique, dynamic simulations must be performed to determine the final configuration.

The configurations found to minimize the approximate effective conductivity are similar to arrangements we would expect if the effective conductivity problem had been solved exactly (see §2.4.3). This shows that the effective potential energy, computed with the point-bubble approximation, is qualitatively correct even when the bubbles become clustered.

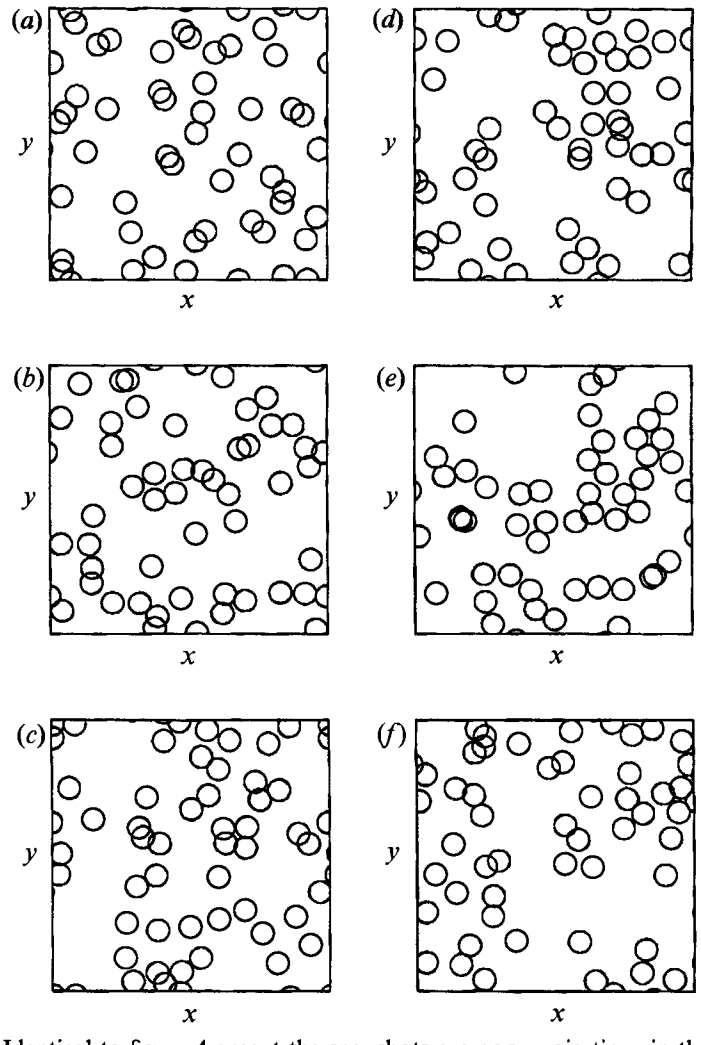

FIGURE 6. Identical to figure 4 except the snapshots are now projections in the (x,y)-plane.

5. Dynamic simulations

5.1. *Outline of the numerical method*

In this section, numerical solutions of bubble trajectories are computed. In order to achieve this it is useful to write (4.6) in the following form:

$$\left.\begin{aligned} \dot{\boldsymbol{u}}_k &= \boldsymbol{F}_k(\boldsymbol{x}_1, \boldsymbol{x}_2, \ldots, \boldsymbol{x}_N, \boldsymbol{u}_1, \boldsymbol{u}_2, \ldots, \boldsymbol{u}_N), \\ \dot{\boldsymbol{x}}_k &= \boldsymbol{u}_k. \end{aligned}\right\} \tag{5.1}$$

This is done by solving the $3N \times 3N$ system for $\dot{\boldsymbol{u}}_k$. In order to evaluate $\boldsymbol{F}_k$, we must compute sums of the form

$$S = \sum_{q=0}^{\infty}{}^{\star} g(\boldsymbol{R}_q), \tag{5.2}$$

where $\boldsymbol{R}_q = \boldsymbol{R} + q\boldsymbol{L}$, $\boldsymbol{q} = (n, m, l)$ and $\boldsymbol{R}$ is the vector joining two bubbles. The exact form of g is determined by (4.6). The lattice sums cannot be evaluated analytically and

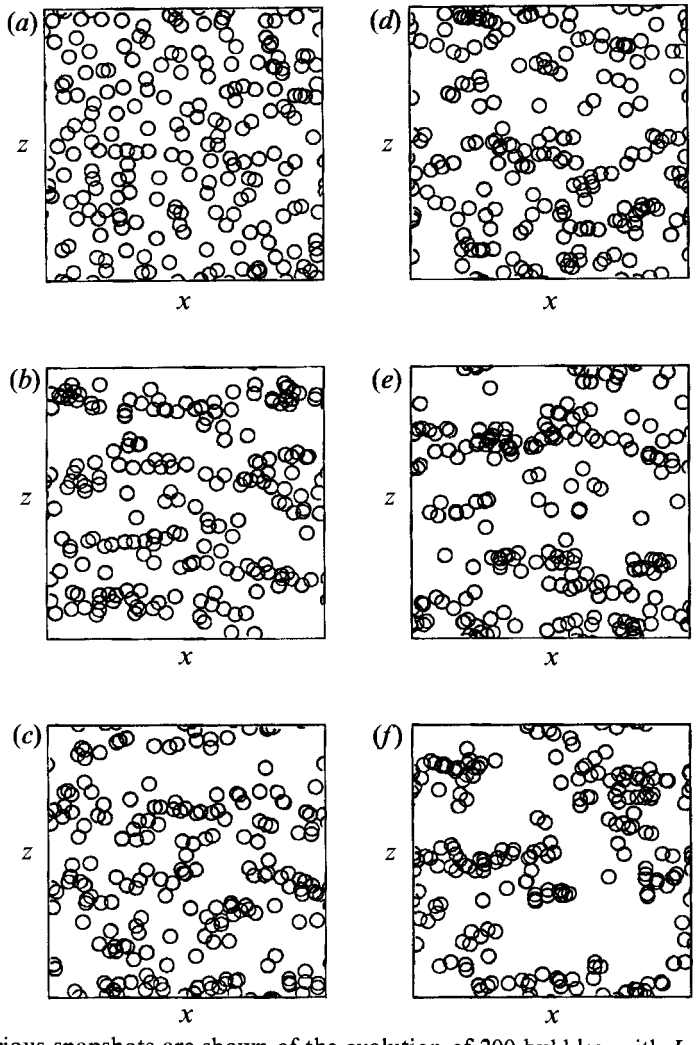

FIGURE 7. Various snapshots are shown of the evolution of 200 bubbles, with $L = 40$. The bubbles are started from a random configuration with unit velocity in the z-direction are shown. This figure presents the projection onto the (x, z)-plane. The snapshot times are: $(a) = 0$, $(b) = 36$, $(c) = 72$, $(d) = 108$, $(e) = 144$, $(f) = 180$.

therefore must be computed numerically. In order to improve the numerical evaluation of (5.2), it is useful to write it as

$$S = \sum_{q=0}^{\infty}{}^{\star} g(R_q^*), \tag{5.3}$$

where $\boldsymbol{R}^* = \boldsymbol{R}_p$ and $\boldsymbol{p}$ is chosen so that $\boldsymbol{R}_p$ is as small as possible. This makes the $\boldsymbol{q} = 0$ term of (5.3) the largest. Numerical evaluation of (5.3) requires a truncation, and we make the following approximation:

$$\sum_{q=0}^{\infty}{}^{\star} \approx \sum_{m=-Q}^{Q} \sum_{n=-Q}^{Q} \sum_{l=-Q}^{Q}. \tag{5.4}$$

We denote the vector field that has been evaluated using the truncated lattice sum by

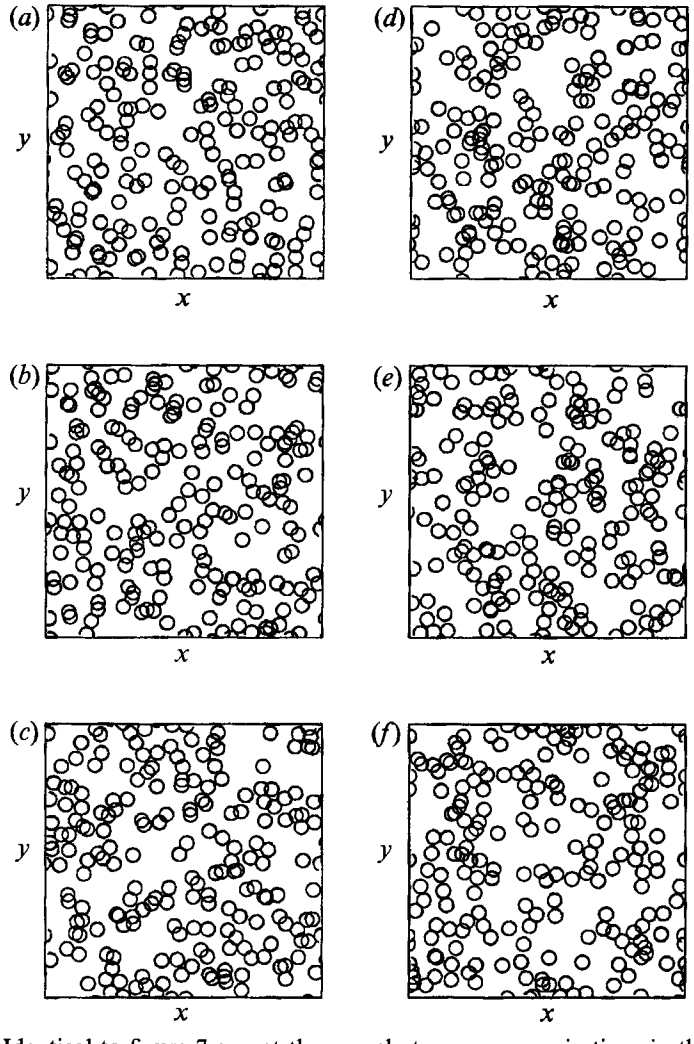

FIGURE 8. Identical to figure 7 except the snapshots are now projections in the (x, y)-plane.

$F_k^{(Q)}$. Since it is very expensive to compute the lattice sums for large values of Q, we will want to keep Q as small as possible without compromising the accuracy too much. To estimate this error we must first have a way of accurately determining F_k. We shall accomplish this using Richardson extrapolation (see, for example, Bender & Orszag 1978, p. 375). We begin by writing (5.4) as

$$F_k = \sum_{Q=1} F_k^{(Q)} - F_k^{(Q-1)}, \tag{5.5}$$

where the terms in the series are found to behave like Q^{-3} for large Q. This suggests that Richardson extrapolation would provide an efficient way of improving the convergence of the sum. Since $F_k^{(Q)}$ are the partial sums of (5.5), Richardson extrapolation gives the following approximation to F_k

$$F_k^* = \sum_{i=1}^{M} \frac{F_k^{(m+i)} (m+i)^M (-1)^{i+M}}{i!(M-i)!}. \tag{5.6}$$

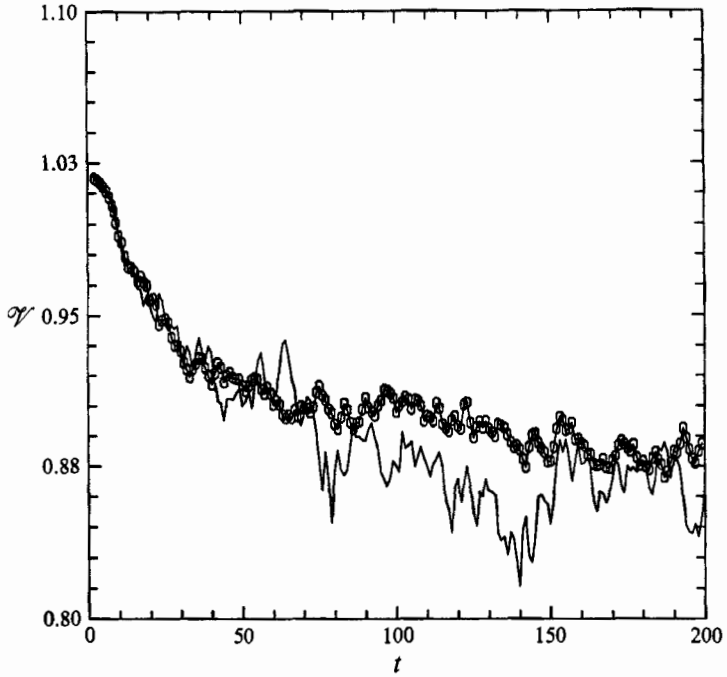

FIGURE 9. A plot of the normalized effective potential energy, $\mathscr{V}$, as a function of time for the numerical results shown in figures 5–8. ——, 50 bubbles; O—O, 200 bubbles. The decrease in $\mathscr{V}$ indicates clustering of the bubbles.

The above expression was examined for a large number of different configurations, having between 20 and 60 bubbles, and was found to converge very quickly. The slowest rate of convergence was observed for random configurations. It was found that F_k^* had converged to at least 8 significant figures for $M = 4$ and $m = 8$ in all of the cases studied. Therefore it was concluded that F_k^* represented a very good approximation to F_k. Unfortunately, using this approximation with $M = 4$ and $m = 8$ would be prohibitively slow for dynamic calculations. Nevertheless, it was observed that $F_k^{(Q)}$ was very close to F_k^* for small Q. More specifically, it was found for a large number of different random distributions that

$$\frac{\sum_k |F_k^{(Q)} - F_k^*|}{\sum_k |F_k^*|} \approx \begin{cases} 1 \times 10^{-2} & (Q = 0), \\ 4 \times 10^{-4} & (Q = 1), \\ 1 \times 10^{-4} & (Q = 2). \end{cases} \tag{5.7}$$

It was also found that any clustering of the bubbles would improve the approximation, therefore the results above represent the worst case possible. In view of the considerable improvement in changing from $Q = 0$ to $Q = 1$, we opted to approximate F_k with $F_k^{(1)}$. The system of ordinary differential equations given by (5.1), with F_k approximated by $F_k^{(1)}$, was solved with a third-order Runge–Kutta–Merson scheme with adaptive time-stepping.

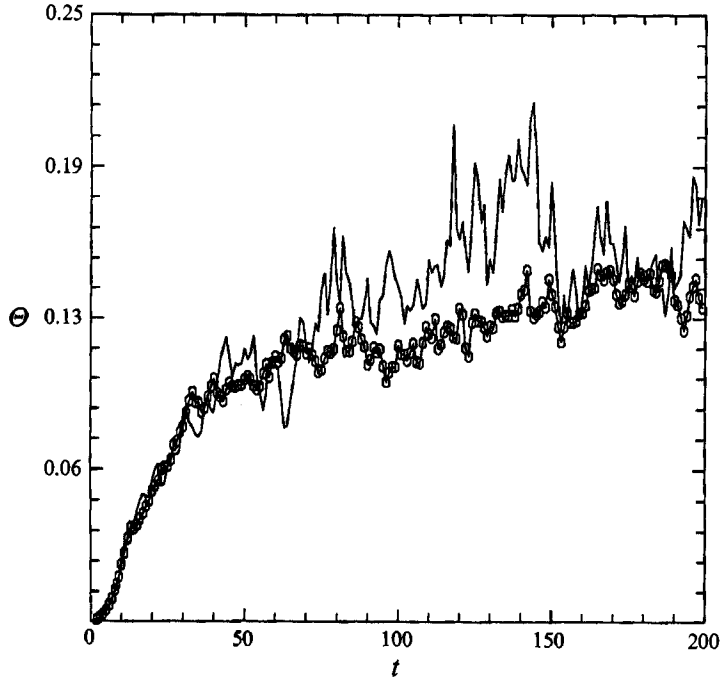

FIGURE 10. A plot of the variance of the bubbles' velocities, Θ, as a function of time, for the numerical results shown in figures 5–8. ——, 50 bubbles; O—O, 200 bubbles.

Before we go on to describe the simulations, let us discuss some quantities that are useful in understanding some aspects of the dynamics. The first is

$$\mathscr{V} = \frac{N\tau}{2V\rho_l}\frac{\boldsymbol{M}^T\boldsymbol{\mathcal{K}}^{-1}\boldsymbol{M}}{\boldsymbol{M}^2}, \tag{5.8}$$

where $\boldsymbol{M}$ is the liquid momentum. $\mathscr{V}$ is the same as $\mathscr{U}$ except that it has been scaled so $\mathscr{V} \approx 1$ for random or periodic mixtures. Smaller values of $\mathscr{V}$ indicate some amount of clustering. Another quantity that is useful is

$$\Theta = \frac{1}{N}\sum_k |\boldsymbol{u}_k - \bar{\boldsymbol{u}}|^2, \tag{5.9}$$

where $\bar{\boldsymbol{u}}$ is the average bubble velocity. This quantity is a measure of how much the bubbles deviate from the mean value. Later we shall see that Θ will behave like a temperature for the collection of bubbles. In the numerical calculations that follow, we shall take $L = 25$ with 50 bubbles and $L = 40$ with 200 bubbles. The void fraction in both cases is close to 0.013. We shall see that the numerical results for $N = 50$ and $L = 25$ are similar to the results when $N = 200$ and $L = 40$. This gives us evidence that the size of the box plays a small role in the dynamics of the bubbles. In the case of $Re = \infty$, the energy and momentum were conserved to 0.1 % and 0.001 %, respectively.

5.2. *Invicid case with no gravity* ($Re = \infty$)

The numerical results of 50 bubbles, started from a random configuration with $\boldsymbol{u}_k(0) = \boldsymbol{e}_z$, are pictured on figures 5 and 6. These figures provide six snapshots of bubble positions projected onto the (x, z)- and (x, y)-planes, respectively. Figures 7

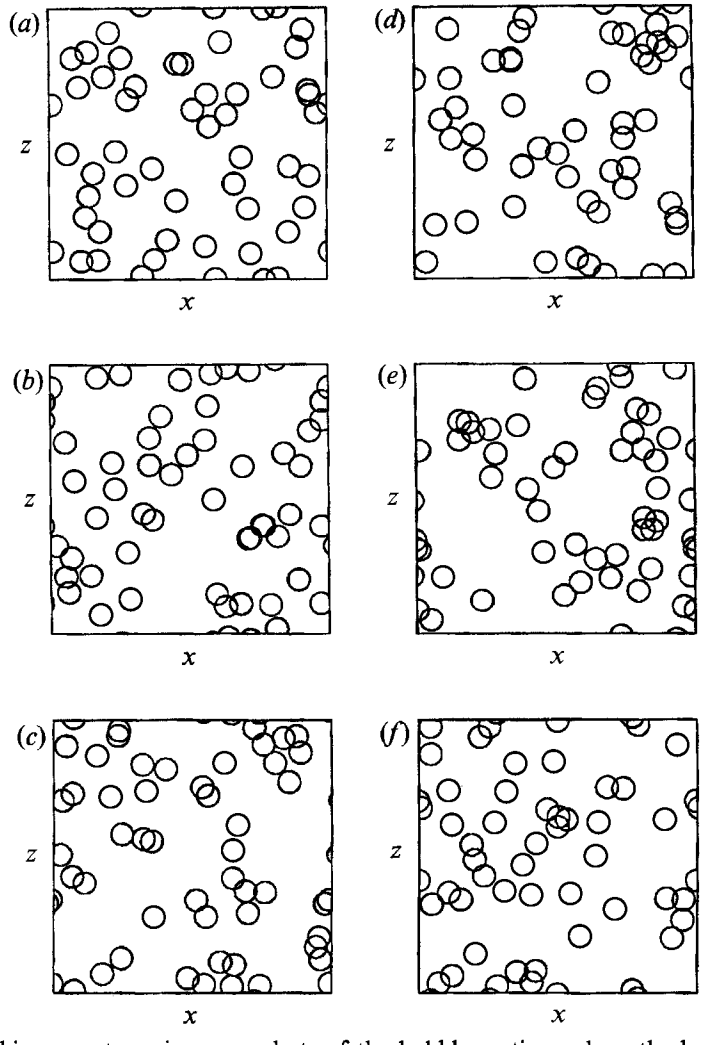

FIGURE 11. This presents various snapshots of the bubble motion, where the bubbles are given a random initial velocity as described by (5.9) with $\lambda = 1.5$. The snapshots are projections in the (x, z)-plane and with the same times as those in figures 5 and 6. The degree of clustering is notably less than that in figure 5. For this simulation $\mathscr{V} \approx 1$; which is consistent with the random configuration observed. Here we have 50 bubbles and $L = 25$.

and 8 present results for 200 bubbles with the same initial conditions as above. These snapshots show the initially random homogeneous configuration of bubbles arranging themselves into flat clusters perpendicular to the z-axis as time increases (the liquid momentum is in the z-direction). The snapshots of projections of the bubbles' position in the (x, y)-plane suggest that they are configured isotropically in this plane. The lengthscales associated with the clusters are approximately the same when $N = 50$ and $L = 25$ and when $N = 200$ and $L = 40$. This indicates that the lengthscales associated with the clustering are not determined by the size of the box.

The behaviour observed here is consistent with the discussion given in §2.4.4 where we argued that the bubbles would try to arrange themselves so as to lower the effective potential energy, $\mathscr{V}$, and at the same time increase the variance of their velocities. Indeed, a plot of $\mathscr{V}$ as a function of time reveals that it decreases from $\mathscr{V} \approx 1$ to

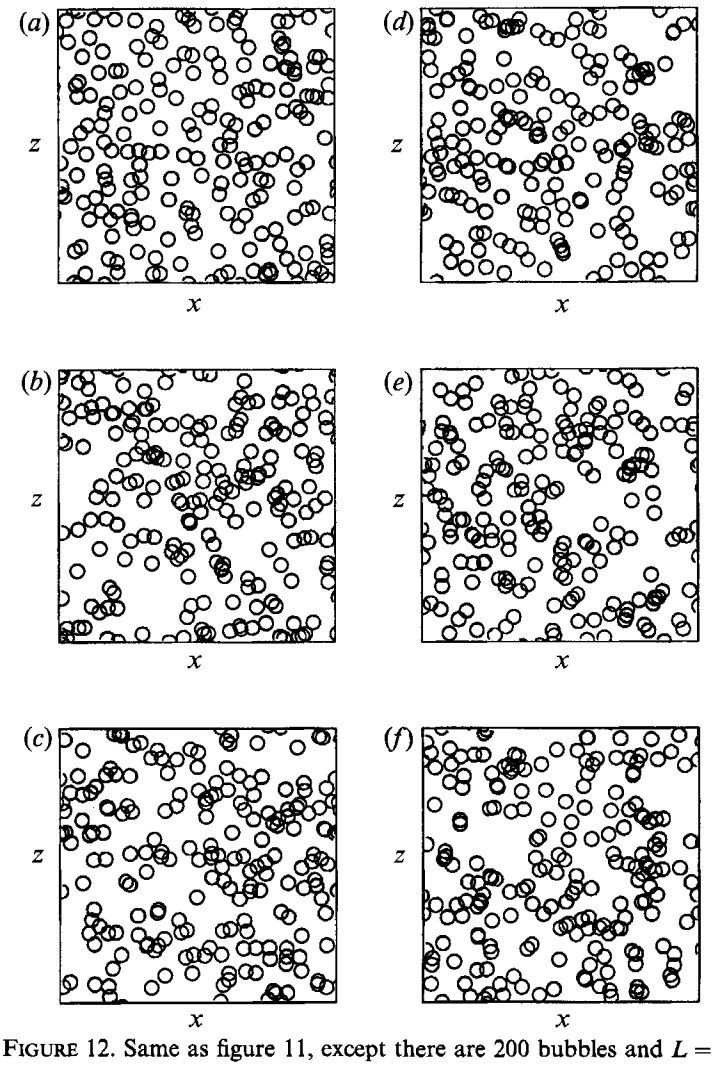

FIGURE 12. Same as figure 11, except there are 200 bubbles and $L = 40$.

$\mathscr{V} \approx 0.88$ during the course of the simulation (see figure 9). On the other hand, figure 10 shows the variance in the bubbles' velocity, Θ, increasing to about 0.14 from zero. Numerical calculations show that if we integrate the system of equations for longer periods of time, $\mathscr{V}$ and Θ will continue to fluctuate at about 0.88 and 0.14, respectively. This suggests that the bubbles have reached a state of statistical equilibrium; however, because of the relatively small number of bubbles, the fluctuations about these equilibrium states is fairly large. Therefore we conclude that these clusters are permanent structures of the bubbly flow and the variance of the bubble's velocity will remain approximately 0.14. The clumps shown on figures 5–8 are not unlike the bubble clumps introduced by Smereka & Milton (1991). They showed that such bubble configurations would give well-posed equations in the variational setting proposed by Geurst (1985).

Now we will consider the situation with the bubbles initially arranged in a random configuration, with initial velocities

$$\boldsymbol{u}_k(0) = \boldsymbol{e}_z + \lambda \boldsymbol{\xi}, \tag{5.10}$$

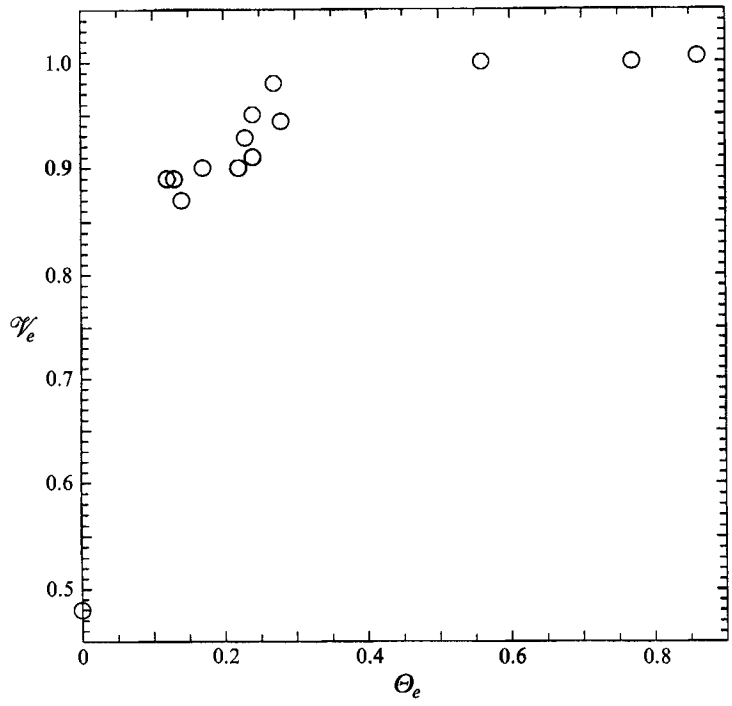

FIGURE 13. $\mathscr{V}_e$ versus Θ_e for 50 bubbles.

where ξ is a random vector whose components are uniform on $[-0.5, 0.5]$ and λ is a parameter which allows the initial value of Θ to be varied. Figures 11 and 12 show six snapshots of the bubbles' position projected on the (x,z)-plane for $\lambda = 1.5$. We have $N = 50$ and $L = 25$ in figure 11, and $N = 200$ and $L = 40$ in figure 12. Clearly, there is almost no clustering of the bubbles, suggesting that the random configuration of bubbles is at statistical equilibrium. In this case, the equilibrium values of the effective potential energy, $\mathscr{V}_e$, and the variance in the bubbles' velocity, Θ_e, were found to be 1.00 and 0.75, respectively. These results suggest that the type of configuration at statistical equilibrium is related to Θ_e.

The relationship between the values of $\mathscr{V}$ and Θ at statistical equilibrium, denoted as $\mathscr{V}_e$ and Θ_e, respectively, is explored through several numerical experiments. In these simulations we consider only $N = 50$ and $L = 25$, with the bubbles initially arranged in a random configuration with initial velocities given by (5.10) (λ is varied for each run). The results of these simulations are summarized in figure 13 where $\mathscr{V}_e$ is plotted as a function of Θ_e. The value of $\mathscr{V}_e$ for $\Theta_e = 0$ is $\min \mathscr{V}_e$ by virtue of the results in §2, and was computed using the method outlined in §4.2. This plot demonstrates that $\mathscr{V}_e$ is related to Θ_e. For Θ_e sufficiently large, $\mathscr{V}_e \approx 1$, consistent with a random arrangement of bubbles. In other words, a random homogeneous configuration of bubbles is stable provided that the variance of their velocities is sufficiently large.

The above calculations suggest an interesting analogy, that Θ_e is akin to a temperature and the collection of bubbles could be considered a gas. As the temperature of the gas is lowered it condenses and the condensed phase will consist of bubble clusters.

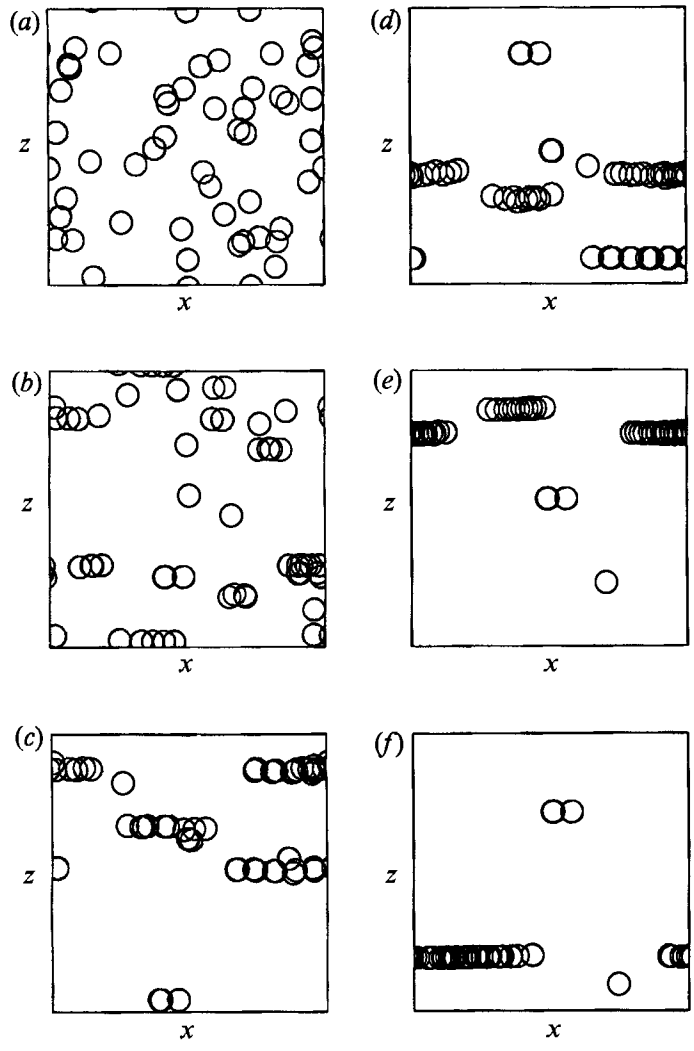

FIGURE 14. Various snapshots are shown of the evolution of 50 bubbles. The bubbles started from rest in a random configuration with (Re = 180). This figure presents the projections onto the (x, z)-plane. The snapshot times are: (a) = 0, (b) = 50, (c) = 100, (d) = 150, (e) = 800, (f) = 1600.

5.3. *Effects of gravity and liquid viscosity* ($Re \neq \infty$)

Presented in figures 14 and 15 are numerical computations for 50 bubbles and Re = 180, which corresponds approximately to a bubble of radius 0.044 cm in water. The bubbles were started from a random configuration with zero velocity. The results contained in these figures clearly show the bubbles clustering in planes perpendicular to the z-direction as time increases. This is similar to behaviour predicted in §2.5 with a one-bubble model for the liquid viscosity, whereas here we have a two-bubble model. Structures similar to these clusters have been observed in fluidized bed experiments by Singh & Joseph (1993). Many experiments in bubbly flow have not reported such phenomena, indicating that the time required for clustering is long, the effect of liquid turbulence may be important or that the variety of bubble sizes is significant.

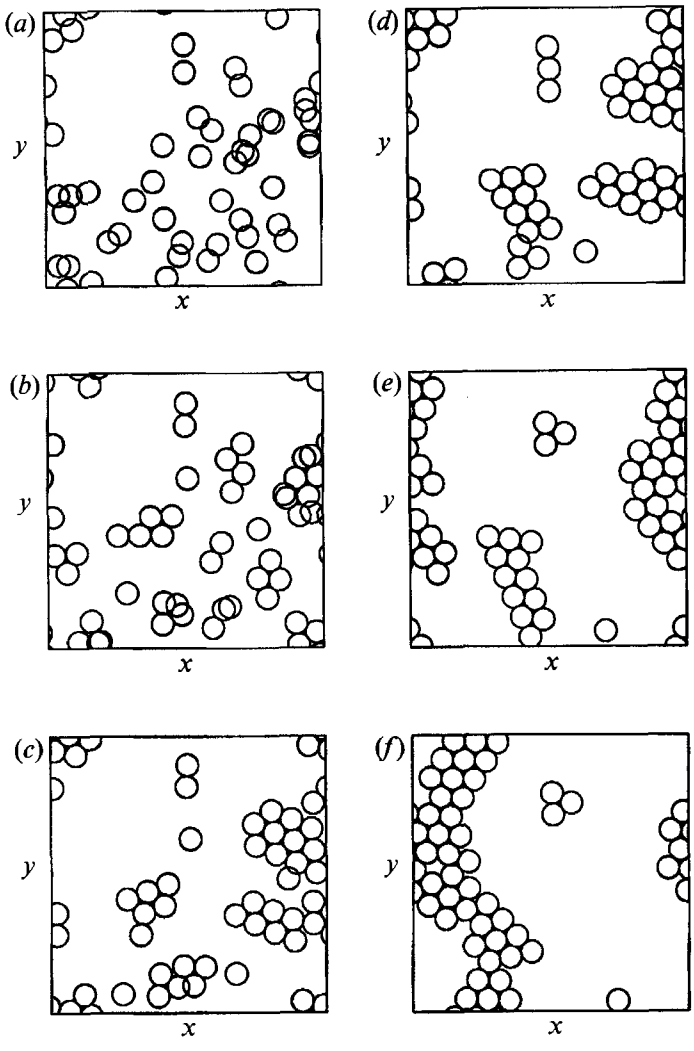

FIGURE 15. Same as figure 14 except the snapshots are now projections in the (x, y)-plane.

6. Summary

The results of this paper show that the type of bubble configuration which is statistically in equilibrium in an inviscid liquid, is related to the variance of the bubbles' velocities. If the variance is small then a random isotropic arrangement of bubbles is not stable and they are observed to cluster. These clusters tend to be pancake-shaped and are oriented broadside to the flow. The bubbles' tendency to organize themselves in this manner is a reflection of a basic variational principle: stable configurations maximize the virtual mass or equivalently minimize the effective conductivity when the variance of velocities is small. On the other hand, a random isotropic arrangement of bubbles will persist, provided the variance of the bubbles' velocities is sufficiently large. This suggests that the effect of liquid turbulence may inhibit clustering, since it would increase the velocity variance of the bubbles. The clustering behaviour is enhanced by the effects of gravity and liquid viscosity and the long-time behaviour results in the formation of flat clusters perpendicular to the direction of gravity.

The author would like to thank B. Brown and R. Caflisch for reading over the manuscript. This research was conducted at both The Institute of Mathematics and its Applications and the Department of Mathematics, UCLA. At the IMA this work was supported by Air Force grant AFOSR-89-0165, by the Institute for Mathematics and its Applications with funds provided by the National Science Foundation and by the Minnesota Supercomputer Institute. At UCLA this work was supported by the National Science Foundation through a postgraduate fellowship.

REFERENCES

BANERJEE, S. & CHAN, A. M. C. 1980 Separated flow model I. Analysis of the averaged and local instantaneous formulations. *Intl J. Multiphase Flow* **6**, 1.

BASSET, A. B. 1887 On the motion of two spheres in a liquid. *Proc. Lond. Math. Soc.* **18**, 369.

BATCHELOR, G. K. 1967 *An Introduction to Fluid Dynamics*. Cambridge University Press.

BATCHELOR, G. K. 1988 A new theory of the instability of a uniform fluidized bed. *J. Fluid Mech.* **193**, 75.

BEEK, P. VAN 1982 $O(\alpha)$-accurate modeling of the virtual mass effect in a liquid–bubble dispersion. *Appl. Sci. Res.* **38**, 323.

BENDER, C. M. & ORSZAG, S. A. 1978 *Advanced Mathematical Methods for Scientists and Engineers*. McGraw-Hill.

BENJAMIN, T. B. 1987 Hamiltonian theory for motions of bubbles in an infinite liquid. *J. Fluid Mech.* **181**, 349.

BIESHEUVEL, A. & GORISSEN, W. C. M. 1990 Void fraction disturbances in a uniform bubbly fluid. *Intl J. Multiphase Flow* **16**, 211.

BIESHEUVEL, A. & WIJNGAARDEN, L. VAN 1984 Two-phase flow equations for a dilute dispersion of gas bubbles in liquid. *J. Fluid Mech.* **148**, 301.

DELHAYE, J. M. & ACHARD, J. L. 1976 On the averaging operators introduced in two-phase flow modeling. *Proc. 1st OECD/NEA Specialists meeting on Transient two-phase flow, Toronto*, vol. 1, p. 5.

DREW, D. A. & WOOD, R. T. 1985 Overview and Taxonamy of Models and Methods. *International Workshop on Two-Phase Flow Fundamentals*, National Bureau of Standards, Maryland, September 1985.

GEURST, J. A. 1985 Virtual mass in two-phase flow. *Physica* **129**A, 233.

GEURST, J. A. 1986 Variational principles and two-fluid hydrodynamics of bubbly liquid/gas mixtures. *Physica* **135**A, 455.

JEFFREY, D. J. 1973 Conduction through a random suspension of spheres. *Proc. R. Soc. Lond.* **335**, 355.

KOK, J. B. W. 1988 Hydrodynamic equations and effective properties of bubbly flows. In *Transient Phenomena in Muliphase Flow* (ed. N. Afgan), p. 127. Hemisphere.

LAMB, H. 1932 *Hydrodynamics*, 6th edn. Cambridge University Press (Dover edition 1945).

LEVICH, V. G. 1962 *Physiochemical Hydrodynamics*. Prentice Hall.

LHUILLIER, D. 1985 Phenomenology of inertia effects in a dispersed solid-fluid mixture. *Intl J. Muliphase Flow* **11**, 427.

MCPHEDRAN, R. C. & MCKENZIE, D. R. 1978 The conductivity of lattices of spheres I. The simple cubic lattice. *Proc. R. Soc. Lond.* A **359**, 45.

PAUCHON, C. & BANERJEE, S. 1986 Interphase momentum interaction effects in the averaged multifield model. Part I: void propagation in bubbly flows. *Intl J. Multiphase Flow* **12**, 559.

PAUCHON, C. & SMEREKA, P. 1992 Momentum interactions in dispersed flow: An averaging and a variational approach. *Intl J. Multiphase Flow* **18**, 65.

RAYLEIGH, R. S. 1892 On the influence of obstacles arranged in a rectangular order upon the properties of a medium. *Phil. Mag.* **34**, 484.

SINGH, P. & JOSEPH, D. D. 1993 Chaos and structure in two-dimensional beds of spheres fluidized by water. *Intl J. Multiphase Flow* (submitted).

SMEREKA, P. & MILTON, G. 1991 Bubbly flow and its relation to conduction in composites. *J. Fluid Mech.* **233**, 65.

WALLIS, G. B. 1989 Inertial coupling in two-phase flows: Macroscopic properties of suspensions in an invicid fluid. *Multiphase Sci. Tech.* **5**, 239.

WALLIS, G. B. 1990 On Geurst's equations for inertial coupling in two-phase flow. In *Two Phase Waves in Fluidized Beds, Flowing Composites and Granular Media*, Institute for Maths and its Applications, University of Minnesota.

WIJNGAARDEN, L. VAN 1976 Hydrodynamical interaction between gas bubbles in liquid. *J. Fluid Mech.* **77**, 27.

WIJNGAARDEN, L. VAN 1982 Bubble interactions in liquid/gas flows in liquid. *Appl. Sci. Res.* **38**, 331.

WIJNGAARDEN, L. VAN & KAPTEYN, C. 1990 Concentration waves in dilute bubble/liquid mixtures. *J. Fluid Mech.* **212**, 111.